# Design and Optimization of Tunable Matching Networks and Aperture-Tuned Antennas for Mobile Wireless Devices

by

George Mankaruse

A thesis
presented to the University of Waterloo
in fulfillment of the
thesis requirement for the degree of
Master of Applied Science
in
Electrical and Computer Engineering

Waterloo, Ontario, Canada, 2013

## AUTHOR'S DECLARATION

I hereby declare that I am the sole author of this thesis. This is a true copy of the thesis, including any required final revisions, as accepted by my examiners.

I understand that my thesis may be made electronically available to the public.

George Mankaruse

## Abstract

In the current wireless market, users have a high level of expectations regarding the functionalities and services added to their wireless mobile devices. At the same time, they also expect performance to remain optimal. In order to meet users' heightened expectations, the level of integration between different subsystems of wireless radios must increase exponentially to keep pace with the increased demand of functionalities. For example, the current size limitations for mobile wireless devices allow space for only a single antenna, but this antenna must cover dual frequency bands, the first extending from 800MHz to 960MHz and the second from 1710MHz to 2300MHz. Extending the antenna bandwidth to cover the lower edge of the spectrum without increasing the physical size of the antenna is a challenging task. Meanwhile, there is also a demand to decrease antenna size to achieve more compact wireless mobile devices and to free up space for newly added features. One means to achieve these contradicting requirements is to use impedance tuners to enable a small-sized antenna to cover wider range of frequencies. In this thesis, we investigate some methods of applying impedance tuners. First, we conduct a comprehensive study on the tuning range of multiple network topologies, after which we present a design method to substitute impractical and expensive variable inductors with practical and relatively inexpensive fixed inductors connected to variable capacitors. These serve as building blocks for impedance tuners. This is followed by a performance investigation of a readily available tunable capacitor. The equivalent circuit is extracted at different bias voltages and across the frequency range of interest. This circuit model is used in the fourth part of this thesis as an input to the simulator. Next, we conduct multiple simulation runs to demonstrate the major differences between two methods of impedance tuning: a tunable matching network and an aperture-based antenna tuning. The simulation results demonstrate the performance limitations of each technique. Finally, we verify the study findings by measurements in an anechoic RF chamber, discovering that the conducted measurements conform to the obtained simulation results.

**Acknowledgements**

I would like to thank my supervisor, Professor Raafat Mansour, for his guidance and support during the course of this research. His technical directions and help with simulation tools, design, and optimization techniques were a great inspiration. Working with Professor Mansour has been a huge benefit to my technical career.

Besides my supervisor, I would also like to thank Professor Omar Ramahi and Professor Nagula Sangary for reading my thesis. Including me in their busy schedule is truly appreciated.

My gratitude also goes to my wife, Mary, and my children, Abraam and Sophia. Their support and understanding during the course of my degree were immeasurable.

Many thanks go as well to my dear friend, Dr. Albert Wasef, for his help and encouragement. His assistance in finishing this thesis was immense.

Finally, I also wish to thank my manager, Mr. Perry Jarmuszewski, for all his support, encouragement and technical guidance which I deeply appreciate.

## Table of Contents

## List of Figures

## List of Tables

# Chapter 1
# Introduction

The integration of wide band radios into consumer electronics has become the driving force in today's high technology markets. Users' expectations of handheld devices have gone far behind the basic requirement of making voice calls with good voice quality. In the 1980s, voice and simple texting were the main functions of a mobile wireless device, but new technologies such as Long Term Evolution (LTE), WiFi, and WiMax have enabled handheld devices to bring the full power of the Internet anywhere to users. Researchers continue to discover new techniques to enhance user experience within the current limitation of physical size, battery life, processing power, heat dissipation, and the addition of frequency bands that need to be covered by handheld wireless devices.

To improve user experience, there are observable and hidden parameters. Observable parameters are increasing download speed, enhancing user interface, display resolution, touch panel responsiveness, etc. Hidden parameters include performance criteria that need to be optimized, such as battery life, transmitter linearity, transmitter efficiency, receiver sensitivity, and so on. Although users usually do not notice these hidden parameters, download/upload speed and link quality are directly related to hidden performance criteria. Therefore, hidden parameters can significantly influence user experience.

In order to guarantee satisfactory performance, wireless devices have to be certified by passing regulatory requirements. Such requirements can be specific for wireless carriers such as PTCRB [1] (PTCRB used to refer to Personal Communication Services Type Certification Review Board) or government agencies such as Federal Communication Committee (FCC) and Industry Canada (IC). These specifications exist to measure hidden performance parameters.

One of the basic challenges in the wireless industry is that network performance is directly related to the maximum linear power that can be transmitted from mobile devices registered on a

network. This is limited by RF power sources (i.e., the current technology of RF power amplifiers available in the industry) and also by physical size restrictions, as the current trend of making slimmer gadgets allows little space for the antenna. Receive performance also plays an important role, especially in the presence of noise, which is directly related to the characteristics of the antenna.

The work presented in this thesis focuses on the optimization of wireless device antenna through exploring different tuning techniques, namely tunable matching networks and tunable antenna apertures.

# 1.1 Motivation

An effort to explain the motivation for this work, we start by detailing the specifications that regulate the industry, followed by a discussion of the RF design challenges of handheld wireless devices. We focus on the design challenges of the antenna [2] and the effect of the surrounding environment changes on the antenna impedance [3]. Based on all of these facts/challenges, the motive of this work is derived.

## 1.1.1 Better Understanding of Specifications

In order to better understand the regulatory specifications, one has to understand why such specifications exist. The enforcers and their motivations are discussed below.

The enforcers of the specifications can be divided into three categories. The first category is government authorities such as the FCC (Federal Communication Commission) in the United States and the IC (Industry Canada) in Canada. The second category is the Industry Enforcement Entities. These entities oversee the device certifications for a range of carrier networks, for example, PTCRB certification [1] in North America, and the Telecommunication Testing and Approval Forums or TAF organization in China [4]. These organizations are in charge of issuing valid International Mobile Equipment Identification numbers (IMEI) for manufacturers that have passed their criteria.

The third category is wireless carriers, who can enforce their own carrier specifications and requirements. Carriers mandate the passing of certain specifications promoting certain devices on their networks and allowing the branding of their networks to be added to the devices' portfolios [5].

The motivations are different for each enforcer. For instance, the FCC in the US mainly enforces specifications related to spectrum efficiency and public safety. They are interested in practical measures that prove that radio can coexist with many other radios. Hence, they are concerned with measurements of spectrum growth due to the modulation of an RF carrier, as well as spectrum growth due to the switching of an RF carrier and the radiated harmonics into other bands [6] [7]. They are also interested in public safety, through measuring exposure to radiation, e.g., Specific Absorption Rate (SAR).

Coexistence with other radios is important with the current trend, where jamming many radios into one single printed circuit board is a standard practice. If we focused solely on the third harmonic of the GSM 850, we would find that it falls in the band of the WiFi radio. Thus, if the level of this harmonic is high, it can jam the WIFI radio receiver in its vicinity, causing a blocker that cannot be mitigated with filtering. The passing level of the harmonics is usually at -30 dBm or -63 dBc [8].

Carriers and industry partner organizations are mainly interested in specifications related to radio firmware and cell coverage. Device RF performance is a major factor in achieving better cell coverage. On the receive side, the sensitivity of the device can determine the minimum amplitude of an RF signal that can be detected by the radio. On the transmit side, the power of the transmitted signal along with the quality of the transmitted signal can determine how many base stations can detect signals from the device.

In this work, the measurements known as Total Radiated Power (TRP) and Total Isotropic Sensitivity (TIS) will be studied. These specifications are known in the industry as Over-the-Air (OTA) measurements.

### 1.1.2 Wireless Radios: Over-the-Air (OTA) Measurements – Receiver

The carriers are mainly concerned with good coverage of their networks. For this reason, there are two measurements of special interest. These measurements are a good indication of the RF performance of handheld wireless devices.

Total Isotropic Sensitivity (TIS) [9] is a swept measurement integrated over a sphere of the device's radiated sensitivity. The measurements are done in an accredited anechoic chamber, where the device is placed on a rotating stand, on a loop back phone call, and rotated to different angles.

A measurement of the effective isotropic sensitivity (EIS) is then recorded and the weighted average is calculated to determine the TIS. Equation (1-1) is used to calculate the TIS [9] [10].

$$\mathrm{TIS} = \frac{2\mathrm{NM}}{\pi \sum_{i=1}^{N-1} \sum_{j=1}^{M-1} \left[ \frac{1}{EIS_{\theta}(\theta_i, \varphi_j)} + \frac{1}{EIS_{\varphi}(\theta_i, \varphi_j)} \right] \sin(\theta_i)}$$

Equation (1-1)

where:

$\boldsymbol{\theta}$ is the vertical angle of the coordinate system, $\boldsymbol{\varphi}$ is the horizontal angle of the coordinate system,

$\boldsymbol{N}$ is theta intervals, $\boldsymbol{M}$ is phi intervals, and $\boldsymbol{EIS_{\theta,\varphi}}$ is the effective isotropic sensitivity at each measurement position.

### 1.1.3 Wireless Radios: Over-the-Air (OTA) Measurements – Transmitter

Total Radiated Power (TRP) [9] is an integration of the average Effective Isotropic Radiated Power over a spherical coordinate system. The same technique used in the TIS measurement is also used to determine the TRP. The average transmitted power is measured at each angle. Equation (1-2) is used to calculate TRP [10] [9].

$$\mathrm{TRP} = \frac{\pi}{2\mathrm{NM}} \sum_{i=1}^{N-1} \sum_{j=1}^{M-1} \left[ EiRP_{\theta}\left(\theta_i, \varphi_j\right) + EiRP_{\varphi}\left(\theta_i, \varphi_j\right) \right] \sin(\theta_i)$$

Equation (1-2)

where $\boldsymbol{\theta}$ is vertical angle of the coordinate system, $\boldsymbol{\varphi}$ is the horizontal angle of the coordinate system,
$\boldsymbol{N}$ is theta intervals, $\boldsymbol{M}$ is phi intervals, and $\boldsymbol{EiRP_{\varphi,\theta}}$ is the effective isotropic radiated power recorded at each angle.

The previous measurements are only meaningful if captured in real life scenarios, such as when a device is held against the face or in a hands-free phone call [11]. Carriers mandate the passing limits for the TRP and TIS when the device is held in these positions. In the next sections, we explain the difficulty in meeting these specifications.

## 1.2 Handheld Devices: RF Design Challenges

Below is a list of points that highlight the main challenges in the RF system design:

- Consumers are pushing for more functions integrated into handheld wireless devices. This requires more radios to be integrated, which increases the bandwidth requirements of mobile device antenna.

- Less space is assigned to the antenna, which means lower antenna efficiency, especially in the lower frequency bands.
- The nonlinearity of the RF power amplifiers under antenna mismatch condition is an extremely challenging issue, especially under mismatch [12].
- Changing of the environment surrounding wireless handheld devices causes changes to the antenna characteristics. This becomes more critical for slimmer devices.
- Faster processors and clock rates cause greater radio density. This results from the harmonics content of the clock, which is usually of a significant amplitude and frequency to cause interference to the wanted signals.

With the demand for smaller and slimmer devices, the physical size of the device is going in the reverse direction of the optimum size required for the antenna, which means that antenna designers are given less space to work with.

Considering all of these challenges, slimmer devices are more likely to be affected by users' handling and interaction with the device. The problem's complexity can be increased exponentially by introducing the nonlinearity characteristics of an RF Power Amplifier (PA).

This puts pressure on handset makers to increase the radiated power from the handheld. An obvious method to improve the performance is to increase the efficiency of the handheld antenna; however, the physical size of the handheld antennas will be a limiting factor. Adaptive Tuning is another method for increasing antenna efficiency. In this thesis, we investigate the application of different tuning techniques in mobile wireless devices.

## 1.3 Thesis Outline

In Chapter 2, a detailed literature review relevant to the area of research is presented, after which a block diagram of multiband wireless radio is discussed to illustrate possible locations for automatic impedance tuners. In Chapter 3, various automatic impedance tuners topologies are presented, followed by a discussion of tuning range and coverage for multiple matching network

topologies. Next, simulation and measurement results for commercially available tunable capacitor are given and then discussed in detail. In Chapter 4, we discuss the concept of Aperture Tuning. Differences between tuning options are presented, along with practical Total Isotropic Sensitivity and Total Radiated Power (TIS/TRP) measurements. In Chapter 5, we conclude this research work and discuss future research directions.

# Chapter 2
# Literature Review

In mobile handsets, there are four main sections that are candidates for impedance tuning [13], [14]

- Antenna matching network
- Power amplifier output and input match
- Filters and diplexers input/output
- Antenna aperture

Fig. 2-1 shows the locations of these tunable networks in a typical mobile wireless handheld device [13].

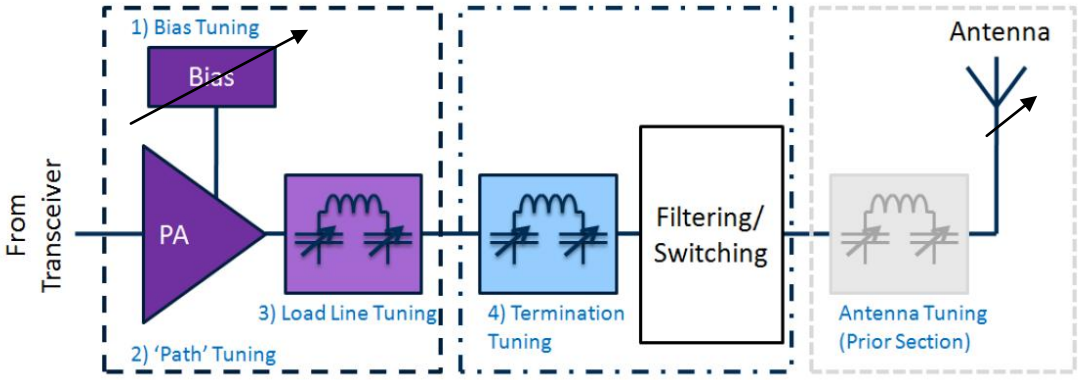


Figure 2-1: Tunable circuits in mobile wireless devices.

Each of these sections has different characteristics and requirements. For example, power handling, linearity and bandwidth can vary significantly at the inputs and outputs of these circuits. This will reflect on the tuning options available.

Also, based on the required location for tuning, the tuning element will be selected. There are multiple tuning elements options listed in Table 2-1 [13]. The specifications of these tuning

elements vary; for example, linearity, tuning range and required DC voltage bias are all parameters that should be considered.

Table 2-1: Tunable elements based on technology.

| Technology | Description |
|---|---|
| Varactor | Diode with voltage controlled capacitance commonly used in standard semiconductor process |
| Voltage Variable Capacitor | Specialized dielectric materials (such as Barium Strontium Titinate **[**BST]) change capacitance values as applied DC voltage changes |
| Micro Electromechanical System (MEMS) Variable Capacitor | Bi State, Voltage Switched capacitors arranged in banks and built using MEMS technology |
| MEMS ohmic switch + MIM Capacitor | MEMS switch selecting Metal-Insulator-Metal capacitor banks |
| Solid State Switch + MIM Capacitor | SOI/SOS/III-V solid state switches integrated with MIM capacitor banks |

In the next section, we review in detail the related work in this area. The review will be conducted based on the candidate circuit that requires tuning.

# 2.1 Tuning the Antenna-Matching Network

As mentioned in Chapter 1, the frequency band of antennas on mobile devices is expanding. In addition, the ‘body effect’ of users increases complexity and promotes unpredictable behavior in the antenna. These challenges drive the need for tunable matching networks. Due to the power

and linearity requirements of mobile wireless handheld radios, MEMS and BST are the potential candidates as tuning elements.

In [15], a tunable MEMS-based matching network was developed. The network was based on a distributed MEMS transmission line. The proposed design has 6561 impedance states and was fabricated on an Alumina substrate. The tuning range was measured for frequencies between 3GHz to 20GHz. The results demonstrated good tuning range in a wide range of frequencies. Fig. 2-2 illustrates the tuning dynamic range of the fabricated circuit.

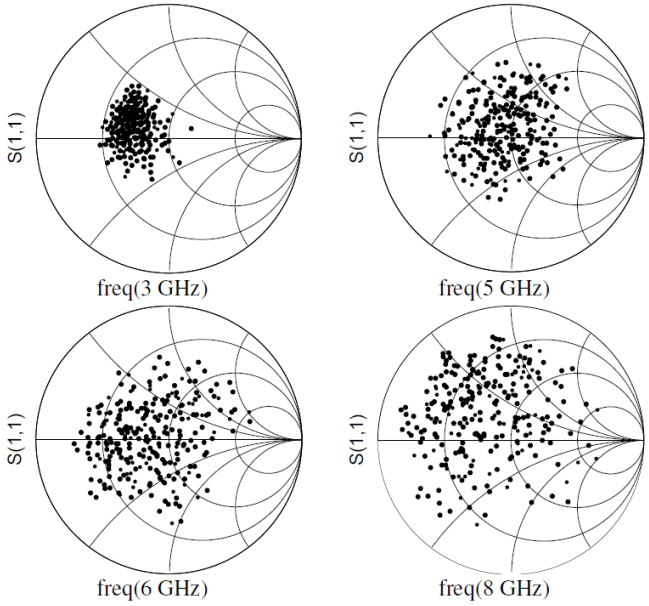


Figure 2-2: Tuning dynamic range of fabricated DMTL [13].

In [16], a single stub MEMS-based impedance tuner was developed. Using the loaded line technique in conjunction with single stub topology showed wide impedance tuning coverage over a wide range of frequencies from 20GHz to 50GHz.

If we refocus our review on lower frequency bands, the work illustrated in [17] is of special interest. In this study, RF MEMS unit cells were used to construct a 5-bit switched capacitor array. RF MEMS capacitive switches were selected due to their high linearity, low-loss, and large tuning range characteristics. The main building block of this tuner was a series LC circuit.

The measured results matched the designed targets. An insertion loss of 0.5 dB, a harmonic distortion below -85dBc, and 10 times tuning range were achieved.

In [18], 5X5 $mm^2$ multi-modes multi-band RF module was presented. The main function of this module was to reverse the effects of antenna degradation due to impedance mismatch. The module was combined with different commercially available phones. The test was done in load-pull setup, and the output power of the test phones was increased by 1.2 dB on average. The proposed design building block was binary weighted RF-MEMS capacitors ranging from 0.75pF to 4.8pF, with a 0.13pF step size. Fig.2-3 shows an example of the tuning strategy. The phase of the load was detected and correction was applied to bring the impedance of the antenna closer to 50 ohms.

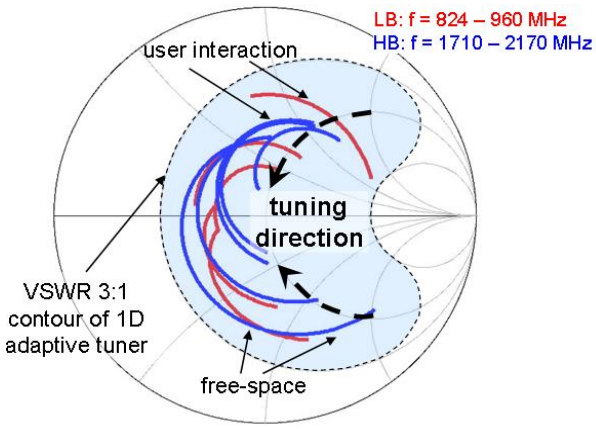


Figure 2-3: Simulated antenna impedance with user interaction [18].

The effectiveness of the proposed design was quantified by simply performing a load-pull measurement to a commercially available phone with and without the tuner. Fig.2-4 shows a comparison of the test results.

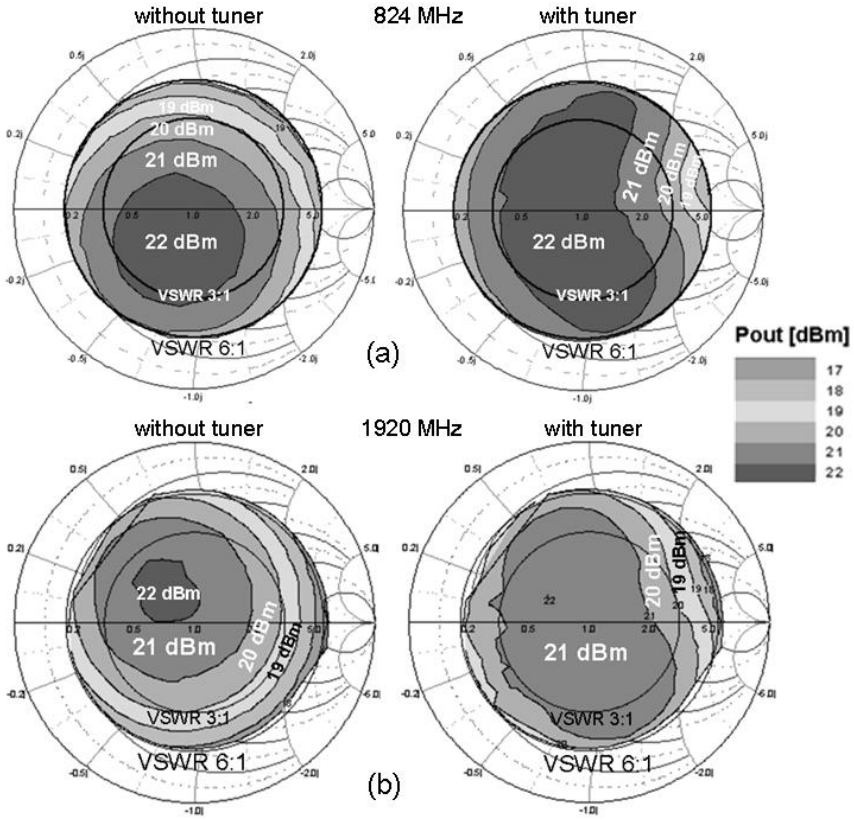


Figure 2-4: Load-pull measurement with and without tuner [18].

Based on the presented results in Fig. 2-4 (a), maximum delivered RF power of 22dBm covered a wider range of load impedances. In Fig. 2-4 (b), the maximum delivered power was reduced from 22 dBm to 21 dBm. However, wider load impedances were covered.

# 2.2 Tuning the RF Power Amplifier Matching Network

Due to the large output power requirements of a mobile handset RF power amplifier (PA) [19] [1] [9], the matching network on the input or output of a RF power amplifier will have different functions and characterizations. The matching network at the output of an RF PA must be able to handle up to 4 watts (36dBm) of power. This is not obvious because, according to European Telecommunications Standards Institute (ETSI) [20], in order to meet power class condition, the

output power of a GSM handset must be calibrated to 2 watts (33dBm). However, the calibration port in this case is at the antenna reference plane, not at the power amplifier output pin.

In order to meet the power requirement at the antenna reference plane, the RF power amplifier must be able to output up to 2.5 watts (34dBm) of power. This is to compensate for the losses in the band-select switch and load variation due to users' interactions with the device.

To illustrate this point, we measured load pull results in Skyworks 77526 RF PA. Fig. 2-5 shows the measurement results. We observed that the maximum power delivered by the PA is not at the 50 ohm load. Hence, if the PA is calibrated at 34dBm, with the load variation the PA output power can reach 35.6dBm.

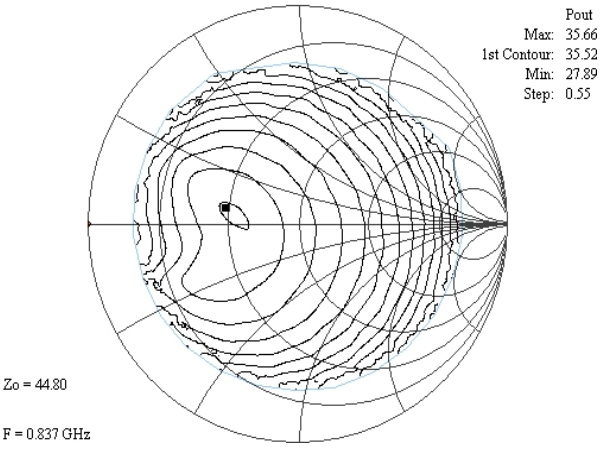


Figure 2-5: Measured load-pull data for Skyworks 77526 RF power amplifier.

In Fig. 2-6 [21], the block diagram of a 2G/3G radio is presented to better understand the function and location of the RF band-select switch. As can be seen, the band select switch is located at the RF power amplifier output. The insertion loss of typical Gallium Arsenide RF switches used in practical handsets is in the vicinity of 1 dB.

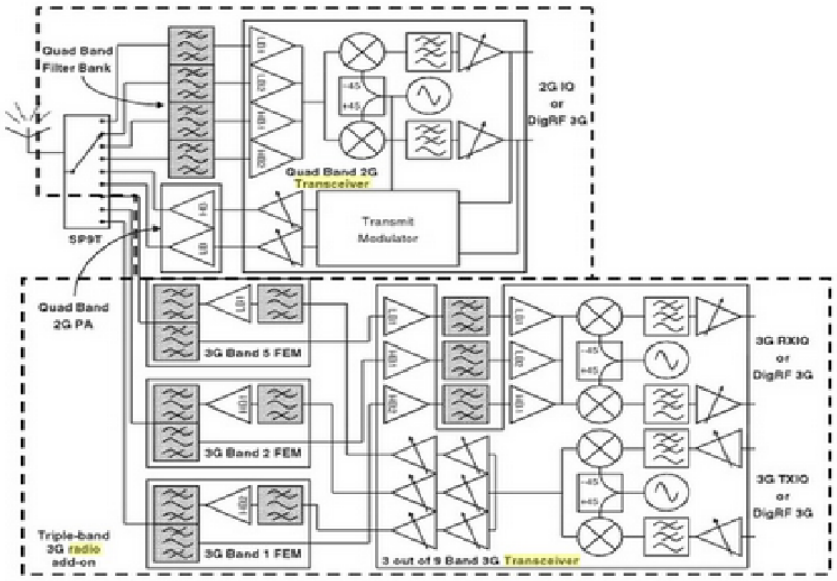


Figure 2-6: 2G/3G radio front-end [18].

Due to large output power requirements, RF power amplifier linearity can be compromised under mismatch conditions, especially if antenna impedance is a moving target, as previously discussed.

The work presented in [12] involved adaptive measures to preserve power amplifier linearity under mismatch. Three adaptive techniques were proposed. By detecting the minimum collector peak voltage, adaptive tuning can change the following parameters:

a) Output power

Fig. 2-7 shows an adaptive output power control loop [12].

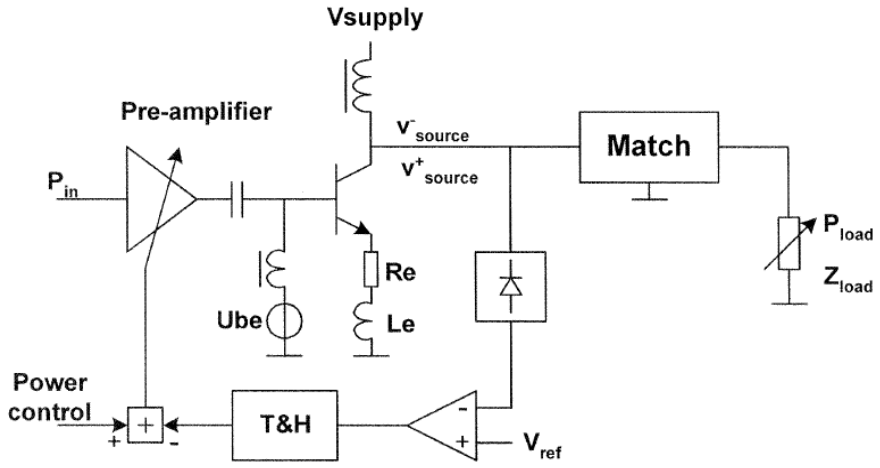


Figure 2-7: Power amplifier output transistor with output power control **[12].**

The peak detect diode is weakly coupled to the transistor collector output stage. The rectified envelop of the output signal is compared to $V_{ref}$. The gain of the pre-amplifier is reduced when the detected RF envelope falls below $V_{ref}$. This will reduce the RF input peak-peak voltage and bring the power amplifier out of saturation.

b) Load line

The load in this case is the antenna of the handheld wireless device. Fig. 2-8 is a simplified circuit diagram of the proposed design [12].

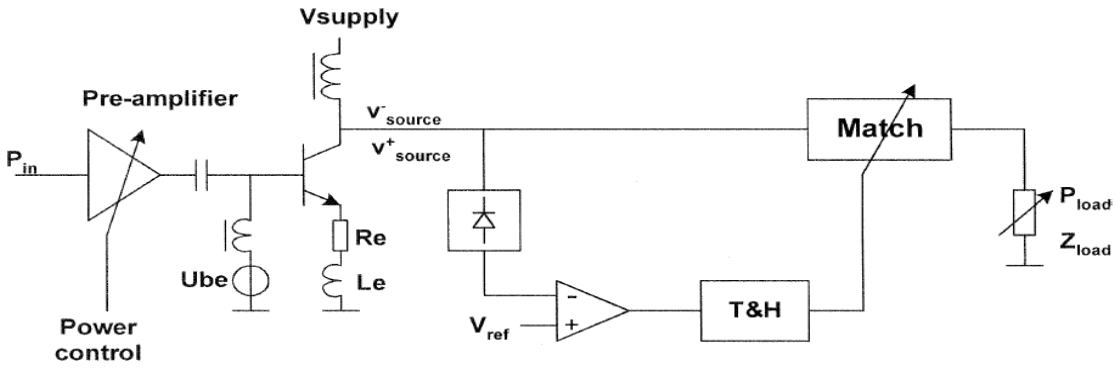


Figure 2-8: Power amplifier with adaptive matching network to prevent saturation **[12].**

When the peak collector RF voltage falls below $V_{ref}$, the power amplifier output match is adjusted to reduce the effective impedance presented to the output stage. This will decrease the peak-to-peak voltage of the RF power amplifier and will prevent saturation.

c) DC bias voltage

Similarly, Fig. 2-9 is a simplified schematic of DC bias control loop [12].

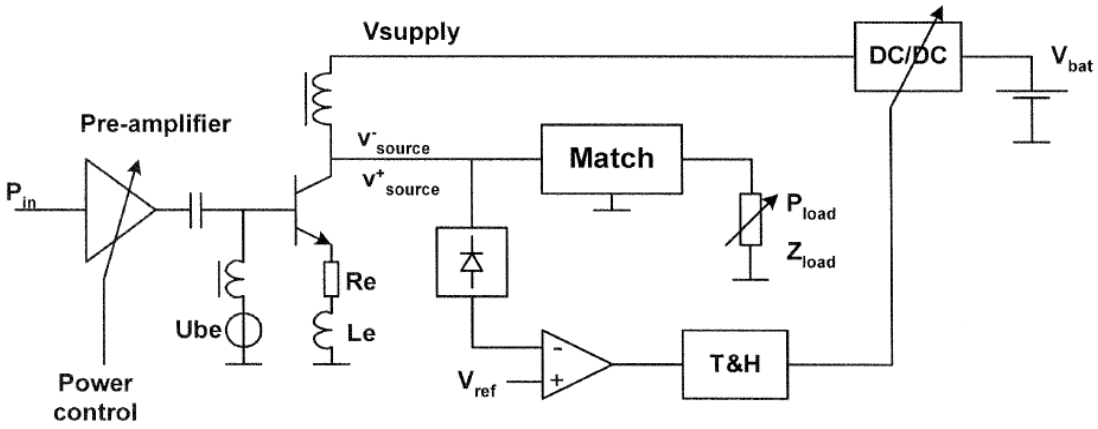


Figure 2-9: DC bias control loop to prevent the saturation of the power amplifier **[12].**

In this configuration, the DC/DC acts as a boost stage for the DC supply voltage. When the saturation condition is detected, the collector supply voltage is up-converted to prevent saturation. The supply voltage in this case can be higher than the rail battery voltage.

The behavior model simulation results for the three discussed methods showed that all three methods can preserve PA linearity under mismatch condition. The easiest and quickest to implement is the output power control loop; however, the drawback with this method is that the maximum output power will be reduced.

The maximum gain can be achieved by implementing the load line adaptive control loop. The linearity of the PA is preserved under mismatch in a similar manner as if an isolator is used

with generally larger output power. The implementation of such a system, however, is dependent on the availability of linear, high quality factor and reliable micromechanical system devices.

## 2.3 Tuning Filters and Diplexer Input and Output Stages

In wireless handset devices, a wide span of RF filters is used. For example, band-stop filters are used at the input of WLAN/WIMAX transceivers to prevent GSM fundamental and harmonics from jamming the receiver. Examples of such filters are LFB212G45SG8A166 and LFB212G49SG8B830, designed by Murata Manufacturing.

Due to the bandwidth and attenuation requirements of such filters, the insertion loss ranges from 1.5 to 2.5 dB. Since most WLAN / WIMAX transceivers are full duplex, the transmit power will also be reduced due to the insertion loss of the filters. This can pose a significant challenge to link budget requirements, which on the other hand increases the need for tunable filters. Due to the low loss, high quality factor, and linearity of RF MEMS [22] [23], they are desirable in such applications.

The work presented in [24] revolved around RF MEMS tunable filters with constant absolute bandwidth. The filter design is based on corrugated coupled lines and ceramic substrates with high dielectric constant ($\epsilon_r$ =9.9 $F.m^{-1}$). The use of high dielectric constant allows for miniaturization of the fabricated design. Two simulation models were built in SONNET. The first model was based on a two-pole wide band tunable filter, and the second model was based on a two-pole narrow band tunable filter. Fig. 2-10 illustrates the layout of the proposed tunable filters [24].

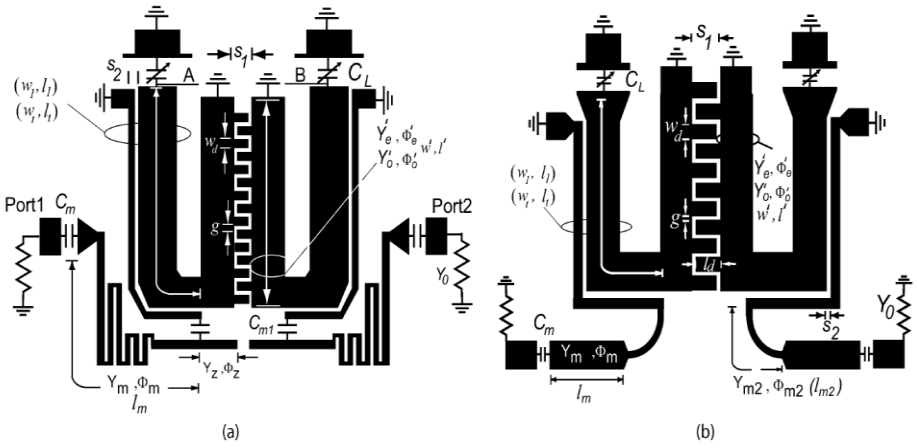


Figure 2-10: Layout of two-pole tunable filter: a) Wide Band; b) Narrow Band **[24].**

The simulation results shown in Fig. 2-11 [24] demonstrate the change in the center frequency with capacitance variations.

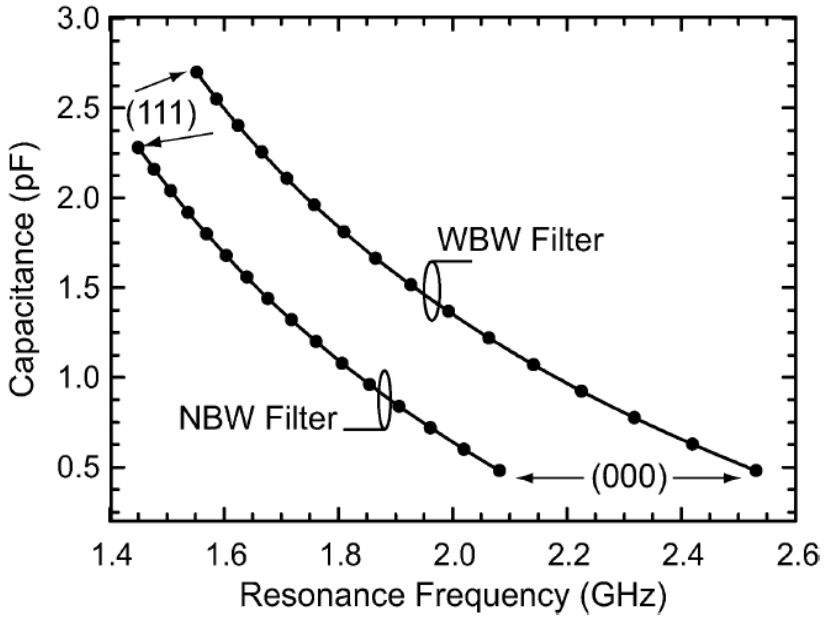


Figure 2-11: Simulated tunable filters center frequency versus loading capacitance **[24].**

An 8-state network was fabricated on a 0.74 mm height substrate, achieving a large capacitance tuning ratio and continuous tuning coverage. Fig. 2-12 shows the fabricated design [24].

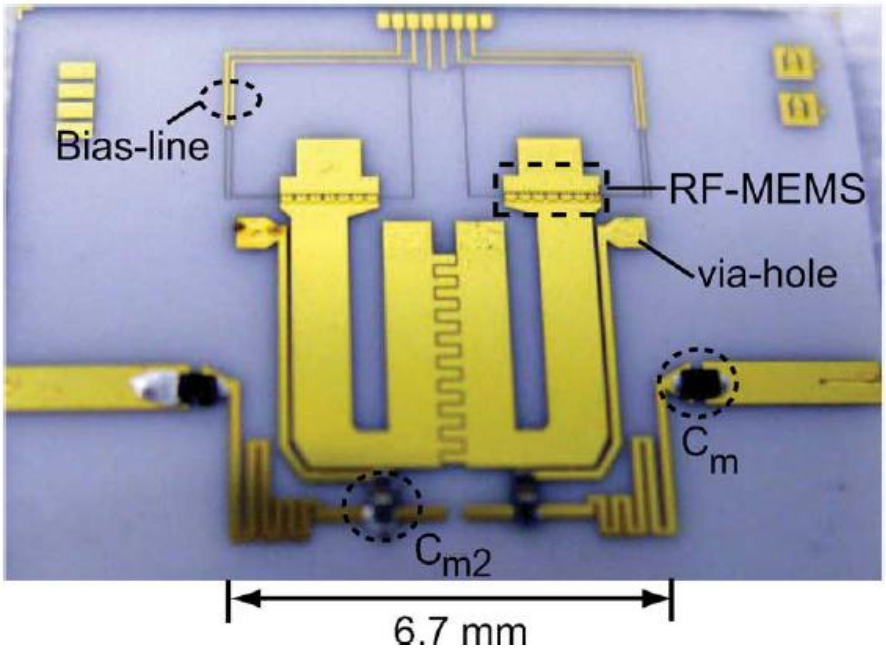


Figure 2-12: Fabricated MEMS wide-bandwidth tunable filter [24].

Table-2 highlights the measured results for both the wide and narrow band tunable filters.

Table 2-2 Summary of the measured RF-MEMS two-pole tunable filter

a) Wide Band Tunable Filter

| $f_o$ (GHz) | 1dB/3dB BW | Insertion Loss (dB) | $f_o$ (GHz) | 1dB/3dB BW | Insertion Loss (dB) |
|---|---|---|---|---|---|
| 1.56 | 104/146 | 2.22 | 2.01 | 123/181 | 1.97 |
| 1.60 | 105/150 | 2.10 | 2.10 | 122/185 | 2.00 |
| 1.66 | 108/155 | 2.10 | 2.13 | 126/186 | 2.00 |
| 1.72 | 114/162 | 2.00 | 2.22 | 126/189 | 2.04 |
| 1.77 | 112/165 | 1.97 | 2.27 | 125/189 | 2.00 |
| 1.82 | 117/169 | 1.94 | 2.34 | 124/188 | 2.00 |
| 1.87 | 119/174 | 1.96 | 2.39 | 120/186 | 2.05 |
| 1.90 | 120/176 | 1.92 | 2.44 | 119/184 | 2.04 |
| 1.94 | 123/178 | 1.92 | 2.48 | 115/182 | 2.03 |

b) Narrow Band Tunable Filter

| $f_o$ (GHz) | 1dB/3dB BW | Insertion Loss (dB) | $f_o$ (GHz) | 1dB/3dB BW | Insertion Loss (dB) |
|---|---|---|---|---|---|
| 1.55 | 69/101 | 1.93 | 1.81 | 75/112 | 1.96 |
| 1.58 | 69/102 | 1.93 | 1.83 | 76/111 | 1.96 |
| 1.59 | 69/105 | 1.92 | 1.85 | 75/112 | 1.95 |
| 1.62 | 71/110 | 1.93 | 1.88 | 75/111 | 1.97 |
| 1.64 | 71/110 | 1.94 | 1.91 | 73/105 | 1.97 |
| 1.66 | 72/110 | 1.96 | 1.93 | 74/112 | 1.97 |
| 1.71 | 73/110 | 1.92 | 1.96 | 73/111 | 1.98 |
| 1.72 | 69/111 | 1.96 | 2.01 | 73/110 | 1.98 |
| 1.78 | 75/111 | 1.92 | 2.04 | 72/109 | 1.99 |

The measured insertion loss for the filter was in the range of 1.9 -2.0 dB. Power handling of 25 dBm with high IIP3 was also verified when the filter introduced no distortion to a wide band CDMA signal of 24.8 dBm of power.

In [25], a tunable band pass filter was developed. The tunable element used was a semiconductor varactor. The design targeted the front-end module of mobile wireless handset devices. The filter could be tuned for DCS, PCS, and UMTS bands.

For miniaturization, a multi-layer Low Temperature Co-fired Ceramic (LTCC) substrate was used. The tuning element was a voltage-controlled dielectric capacitor or Parascan capacitor, which is proprietary technology for Paratek. The tunable capacitor used in this work had a high quality factor (Q), low loss, and high linearity characteristics. These factors promote high power handling capabilities and the possibility of industry utilization, as this filter replaces three fixed band pass filters.

To meet the design requirements, a single zero, three-pole asymmetric filter was used. Fig. 2-13 shows the schematic and layout of the proposed filter [25].The measured results for this

filter showed an insertion loss of 4.3dB across the three bands (DCS, PCS and UMTS). As can be seen, the return loss was better than 15dB across the bands of interest.

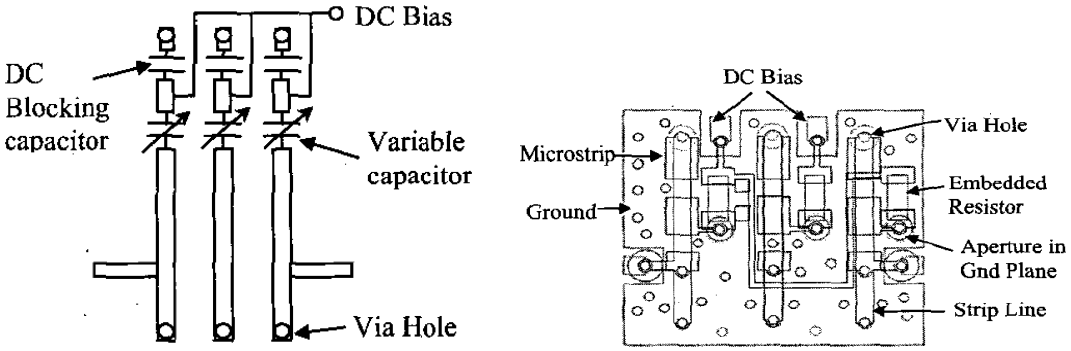


a) Schematic b) Layout

Figure 2-13 3-Pole single zero tunable filter: a) schematic; b) layout **[25].**

# 2.4 Tuning the Antenna Aperture (Aperture Tuning)

Tuning the antenna aperture is based on altering the electrical length of the antenna. This can be achieved by locating the high current routes on the antenna elements. Widely available simulation software would analyze and display the current distribution on the antenna element. High current areas would be suitable candidates for inserting tunable elements [26] in shunt or in a series [14].

In [26], a tunable PIFA was proposed. The antenna can cover the following frequency bands: DCS (1710-1880 MHz), PCS (1880-1990 MHz), UMTS (1900-2170 MHz), WiBro (2300-2390 MHz), WLAN (5.2, 5.8 GHz), Bluetooth (2400-2480 MHz), and ISM band (2500-2700 MHz). The proposed antenna volume is 0.741 $cm^3$, which makes it suitable for integration in handset applications. A varactor diode was selected as the main tuning element. The proposed antenna structure is shown in Fig. 2-14.

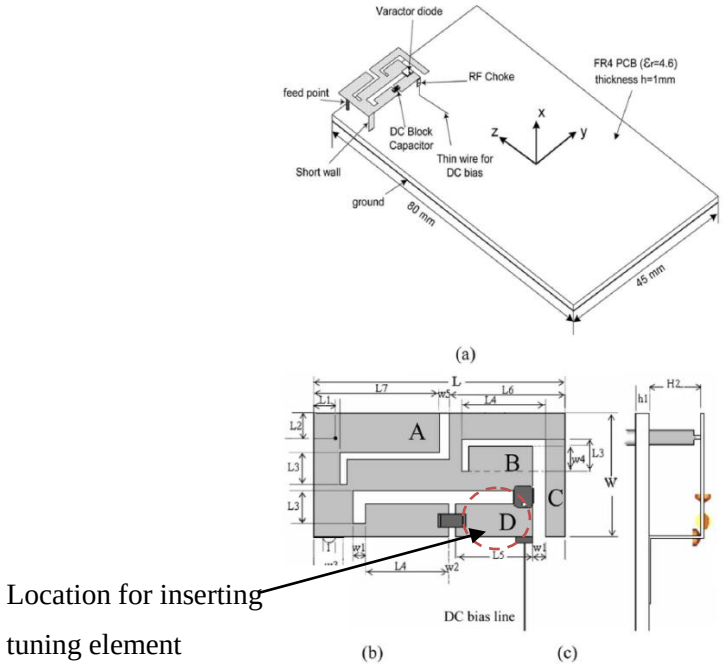


Figure 2-14: Geometry of the proposed antenna: a) 3-D view; b) top view; c) side view **[26].**

Table 2-3: Summary of the design dimensions.

Table 2-3: Dimensions of the proposed antenna.

| Parameter | Value (mm) | Parameter | Value (mm) |
|---|---|---|---|
| L | 19.5 | L1 | 1.45 |
| W | 9.5 | L2 | 1.8 |
| h1 | 1 | L3 | 2.5 |
| H2 | 4 | L4 | 6.5 |
| w1 | 1 | L5 | 6 |
| w2 | 0.5 | L6 | 9 |
| w3 | 2 | L7 | 9.75 |
| w4 | 2 | w5 | 0.75 |

A varactor diode with part number MA46H (manufactured by Ma-Com Technology Solutions) was added to the structure, as shown in Fig. 2-14 (b). The location of the diode was optimized based on the desired tuning frequency. The Microwave Studio Simulation (CST) program was used for location optimization.

The varactor diode specifications are listed in [27], and CST was used to sweep the bias DC voltage of the varactor diode. The return loss of the antenna was captured at several different bias voltages. Fig. 2-15 shows the simulated-versus-measured results for the antenna return loss (S11) [26]. The simulated and measured antenna gains are listed in Table 4.

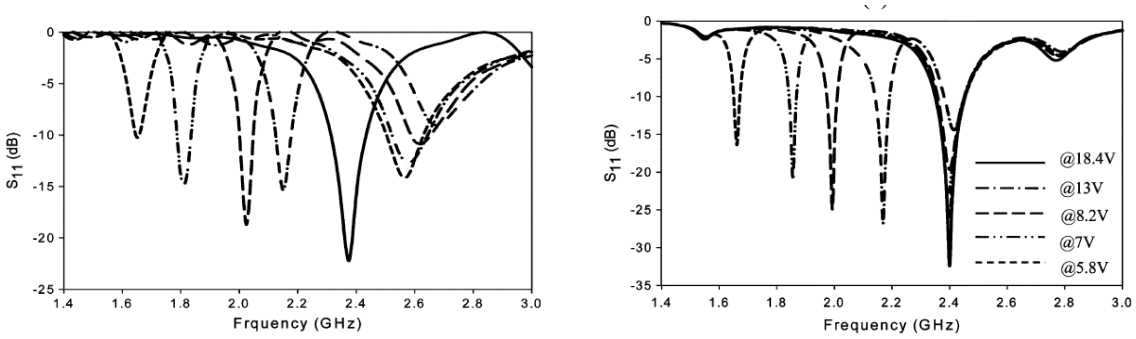


a) Simulated S11 in dB b) Measured S11 in dB

Figure 2-15: Tunable PIFA structure S11 at different bias voltages **[26].**

Table 2-4: The simulated and measured antenna gain.

| Frequency (GHz) | 1.74 | 1.9 | 2.1 | 2.4 | 5.2 | 5.8 |
|---|---|---|---|---|---|---|
| Maximum Measured Gain (dB) | 1.84 | 1.86 | 1.73 | 2.36 | 2.74 | 2.41 |
| Gain (dB) Simulated | 1.4 | 1.7 | 2.1 | 3.78 | 3.8 | 2.6 |

In [14], the author proposed the aperture tuning technique to transform a fixed non-tunable antenna into a smaller tunable antenna. This was achieved by loading the antenna element with different elements, such as inductors and capacitors. Understanding the behavior of the antenna surface current by means of a computer aided simulation was the key to accurate optimization for the tunable elements. Full electromagnetic simulation using Method of Moment (MOM) engine in FEKO was performed on the antenna in order to capture the surface current distribution on the antenna. Based on the simulation results, the position of the tuning element was selected.

Different loading techniques were discussed:

a) Series loading with inductor – shifts the resonance to lower frequency.
b) Series loading with a capacitor – shifts the resonance to higher frequency.
c) Shunt loading with an inductor – shifts the resonance to higher frequency.
d) Shunt loading with a capacitor – shifts the resonance to lower frequency.
e) Loading with L-C circuit.

When loading with a parallel L-C circuit:

$$Z_{lc} = \frac{jwl}{1 - \omega^2 LC}$$

Equation (2-1)

When loading with Series L-C circuit

$$Z_{lc} = \frac{1 - \omega^2 LC}{jwC}$$

Equation (2-2)

The impedance can be inductive, capacitive, or at resonance infinite. However, for increased miniaturization, we need to operate in the inductive region.

Design steps were discussed, as follows:

- Start with a fixed antenna that covers some of the frequency bands of interest. The fixed antenna must have reasonable return loss and radiation efficiency.
- Define the practical loading topology and subsequently define the desired capacitive or inductive loading.
- Using simulation, study the antenna surface current. This will define the loading location at the desired tuning frequency.
- Incorporate the tuning element and start optimization.

The concept was proved on a simple structure and then re-applied on a complex PIFA and IFA antenna.

# Chapter 3
# Tunable Matching Networks

In this chapter, we demonstrate the tuning range of various matching networks topologies, focusing on T and Π topology in both high pass and low pass configurations. We do this is to limit the number of reactive elements to three elements, thus minimizing the losses of the network [28]. In addition, we restrict the values of the reactive elements to those values which are commercially available with reasonable quality factor and physical size. For example, we use capacitor values in the range of 0.5 to 10pF and inductor values in the range of 2 to 12nH. This allows for the practical utilization of the tuning network. We also study the performance of a tunable BST capacitor at a wide span of bias voltage. The quality factor, effective capacitance, and effective resistance of the tunable capacitor are then calculated based on the measurement results.

The following is the work flow for this study:

a) We set up a simulation bench using Agilent Design System (ADS). The value of the reactive element for each network is set as a swept variable in the simulation.

b) We use ideal components and sweep their values to find the maximum tuning range for each network.

c) We illustrate a technique to substitute variable inductors with fixed inductor connected with series/shunt tunable capacitors.

d) We measure the two-port scattering parameters of a commercially available tunable capacitor, with its value selected to be suitable for the frequency band of interest. Based on the measured S-parameters model, we derive the quality factor, effective resistance, and capacitance of the component.

e) We swap the ideal components with the true model of a commercially available BST capacitor and discuss the performance limitations.

## 3.1 Π Topology

### 3.1.1 Low Pass Π Network

Fig. 3-1 illustrates the ADS simulation bench that we developed for the tunable low pass Π network. We will now study the behavior of the network at two frequency bands. The first band is the low band for GSM, which extends from 824MHz to 960MHz, and the second band is the GSM high band, which extends from 1710MHz to 1990MHz [19]. For the low frequency band, the values of the shunt capacitors are swept from 1pF to 7pF, and the value of the series inductor is swept from 4nH to 12nH in 2nH steps. Similarly, for the high frequency band, the values of the shunt capacitors are swept from 0.5 pF to 3.5pF, and the inductor value is swept from 2nH to 6nH in 2nH steps. Fig. 3-2 shows the resulting tuning range of the circuit.

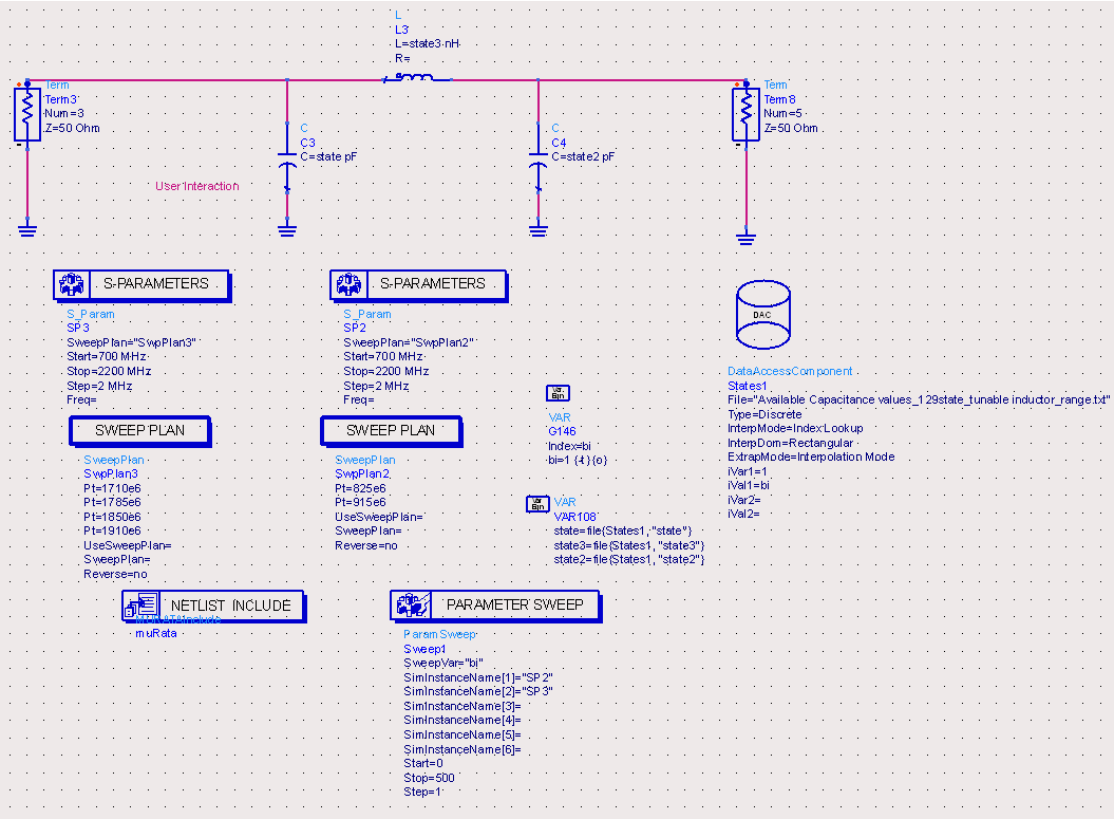


Figure 3-1: ADS simulation bench for tunable low pass PI network.

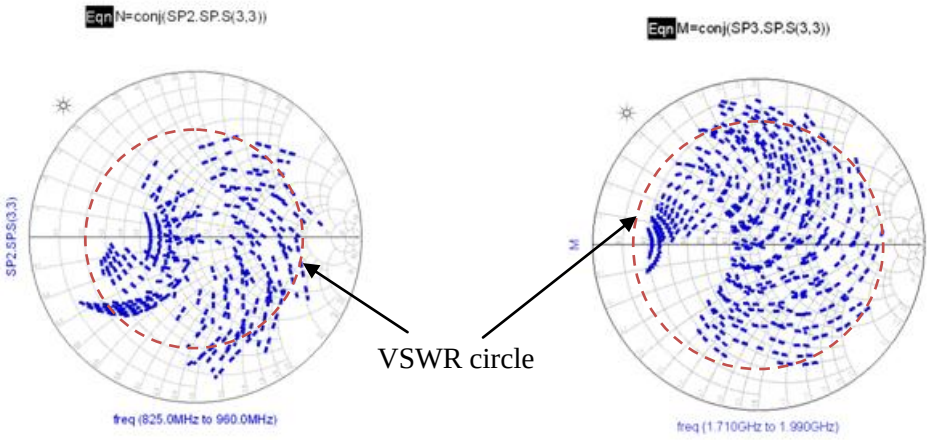


a) Low Band b) High Band

Figure 3-2: Impedance dynamic range for low pass **Π** network.

From Fig. 3-2, we can observe wide impedance coverage for a low pass Π network. From the Voltage Standing Wave Ratio (VSWR) circle, we observe up to 6.5:1 load coverage for the high frequency band and up to 5:1 load impedance coverage for the low frequency band. Same VSWR circle will be used as benchmark to compare other topologies.

## 3.1.2 High Pass Π Network

Similarly, we conducted several simulations on the tunable high pass Π topology in ADS. Fig.3-3 shows the ADS simulation bench that we developed for a high pass Π network. The inductors values are swept from 4nH to 12nH for the low frequency band and from 2 to 8nH for the high frequency band. The capacitor value is also swept from 2 to 8pF for the low frequency band and from 1 to 4 pF for the high frequency bands. Fig. 3-4 shows the resulting tuning range of the circuit.

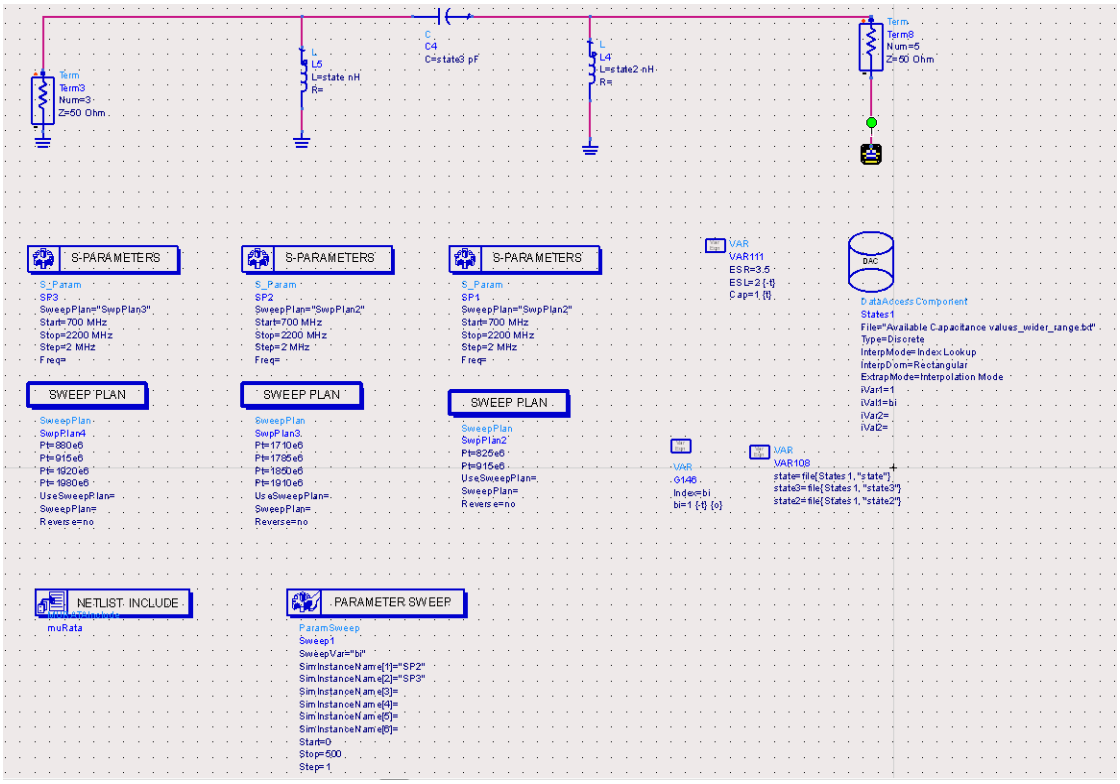


Figure 3-3:ADS simulation bench for tunable high pass PI network.

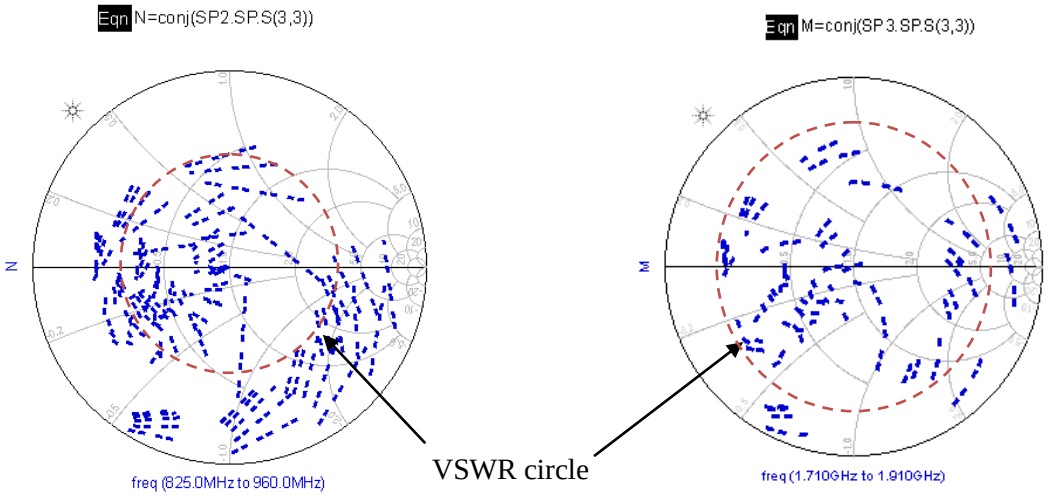


Figure 3-4: Impedance dynamic range for high pass PI network.

From Fig. 3-4, we can observe the impedance coverage for a high pass Π network. From the VSWR circle, we observe up to 6.5:1 load coverage for the high frequency band; however, there

are many spots within the VSWR circle that are not covered. For the low band, the coverage is concentrated more toward the lower end of the Smith chart, which means more capacitive than inductive load impedances can be covered.

## 3.2 T Topology

### 3.2.1 Low Pass T

Similarly, we conducted several simulations on the tunable low pass T topology using ADS, where the developed schematic is shown in Fig. 3-5. The inductor values are swept from 4 to 12nH for the low frequency band and from 2 to 8nH for the high frequency band. The capacitor value is also swept from 2 to 8 pF for the low frequency band and from 1 to 4 pF for the high frequency bands. Fig. 3-6 shows the resulting tuning range of the circuit.

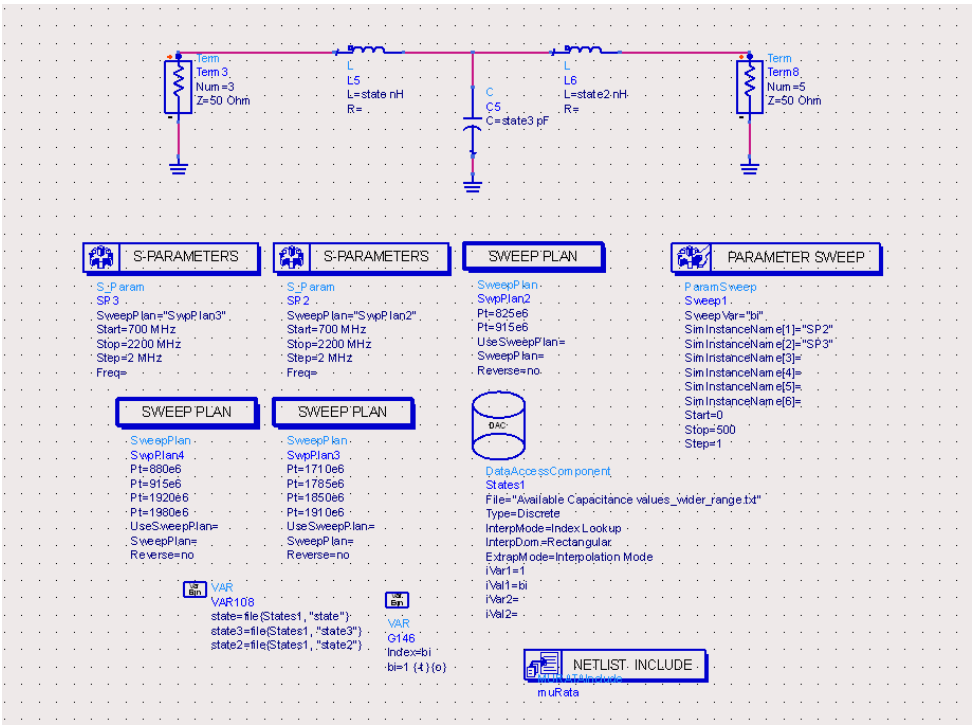


Figure 3-5: ADS simulation bench for tunable low pass T network.

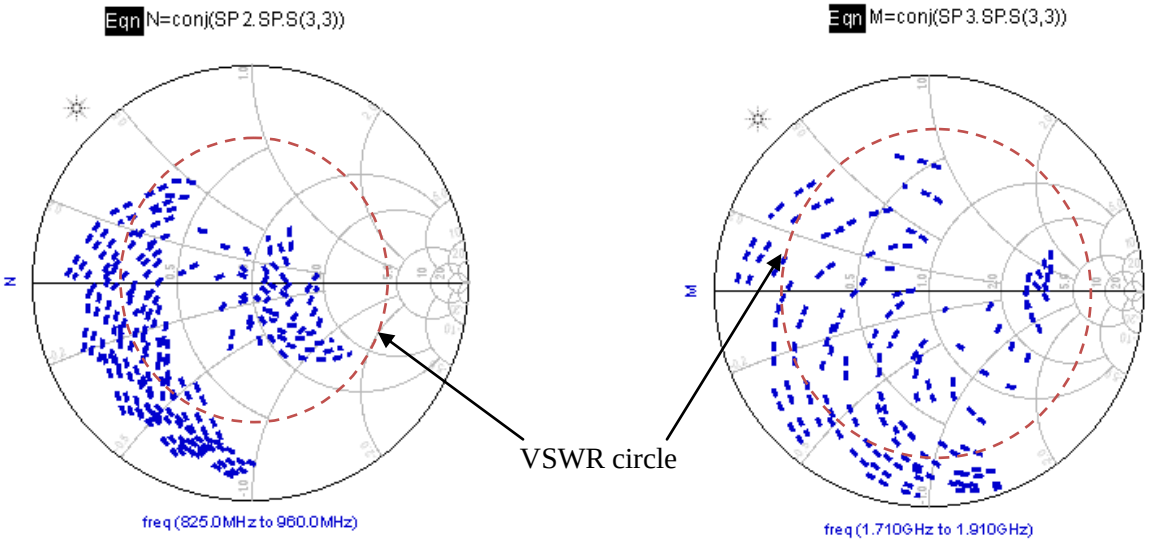


a) Low Band b) High Band

Figure 3-6: Impedance dynamic range for low pass T network.

In Fig. 3-6, we can observe the impedance coverage for a low pass T network. From the VSWR circle , we observed that the covered range of impedances are concentrated more to the left side of the Smith chart, which means that low impedance loads are covered by this network. This is valid for both high and low frequency bands.

## 3.2.2 High Pass T

Similarly, we conducted several simulations on high pass T topology in ADS using the schematic shown in Fig. 3-7. The inductor values are swept from 4nH to 12nH for the low frequency band and from 2 to 8nH for the high frequency band. The capacitors values are also swept from 2 to 8pF for the low frequency band and from 1 to 4 pF for the high frequency bands. Fig. 3-8 shows the circuit's obtained tuning range.

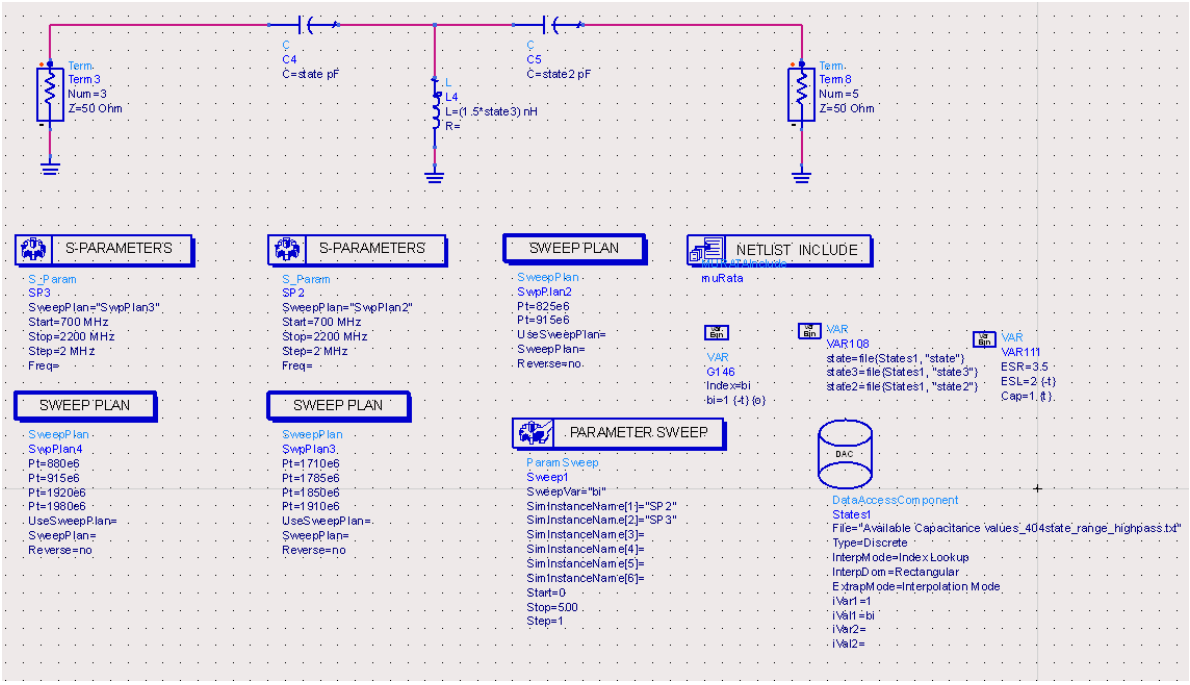


Figure 3-7: ADS simulation bench for tunable high pass T network.

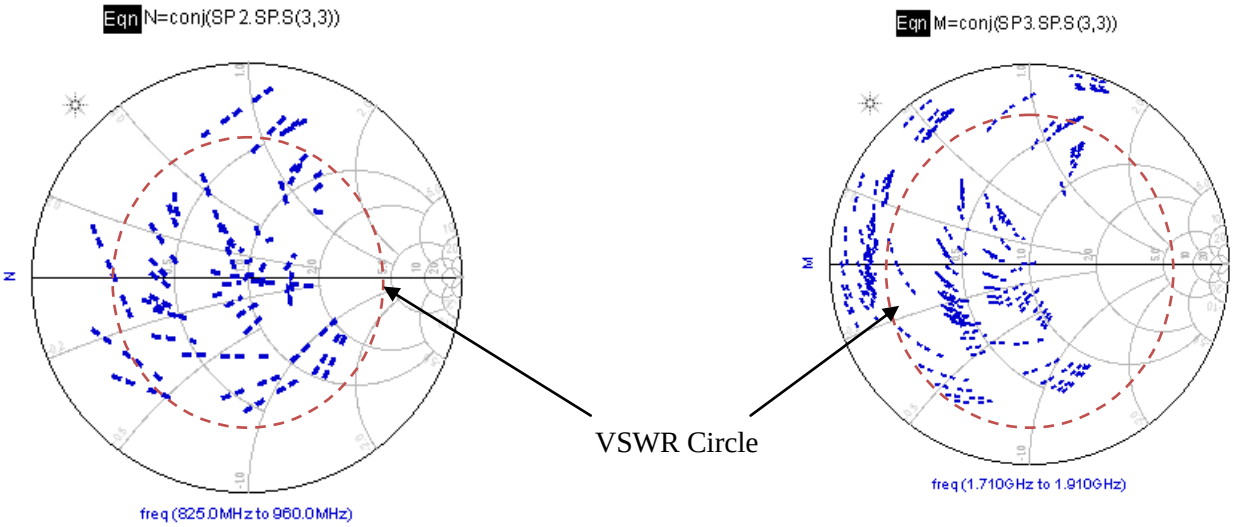


a) Low Band b) High Band

Figure 3-8: Impedance dynamic range for high pass T network.

In Fig. 3-8, we can observe wide impedance coverage for a high pass T network. According to the VSWR circle, there are many spots within the circle that are not covered for the high frequency band. For the low band, however, more impedance values are covered within the VSWR circle.

## 3.3 Technique of Practical Implementation of Tunable Inductors

Based on the results obtained in sections 3.1 and 3.2, we can conclude that the tuning range of the Π network is more suitable for practical utilization, as it covers a wider range of load impedances within the bench mark VSWR range.

Consequently, we will focus on the Π network with the least number of inductors, because it is generally difficult to find tunable inductors that meet size and performance restrictions. Although an RF switch is used to connect different values inductors in and out of the circuit, the use of the switch is undesirable due to added insertion loss, non-linearity and isolation issues, which indeed can make the commercialization of the impedance tuner less attractive. Accordingly, we will use the low pass Π network as the main building block for the proposed impedance tuner.

In order to substitute for the variable inductor, a combination of variable capacitors is connected with a fixed value inductor. Fig. 3-9 shows the schematic of the proposed circuit.

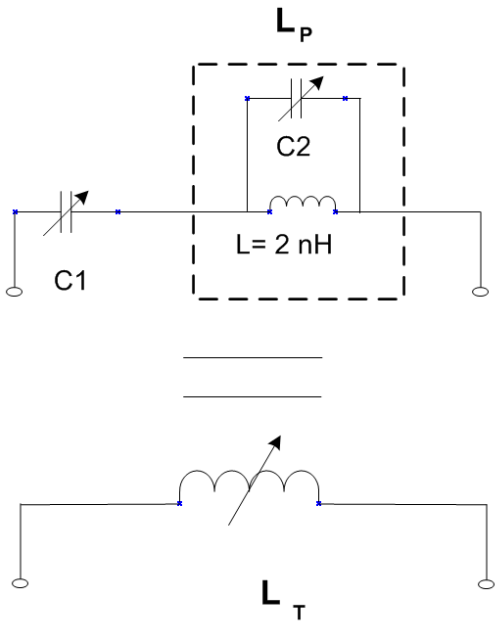


Figure 3-9: Variable inductor using tunable capacitor.

The equivalent impedance of the series ($L_p$-$C_1$) circuit $Z_s$ can be calculated as:

$$Z_s = j\omega L_P + \frac{1}{j\omega C_1} = \frac{1 - \omega^2 L_P C_1}{J\omega C_1}$$

Equation 3-1

Therefore:

$$Z_s \; is \;\; capacitive \quad C = \frac{C_1}{1 - \omega^2 L_P C_1} \quad When \;\; \omega < \frac{1}{\sqrt{L_P C_1}}$$

$$Z_s \; is \; inductive \quad L_T = \; L_P - \frac{1}{\omega^2 C_1} \quad When \;\; \omega \; > \frac{1}{\sqrt{L_P C_1}}$$

Equation 3-2

Similarly, the equivalent impedance of the parallel (L-$C_2$) circuit $Z_p$ can be calculated as:

$$Z_p = \frac{j\omega L * \frac{1}{j\omega C_2}}{j\omega L + \frac{1}{j\omega C_2}} = \frac{J\omega L}{1 - \omega^2 L C_2}$$

Equation 3-3

$$Z_p \; is \; inductive \quad L_P = \frac{L}{1 - \omega^2 L C_2} \quad When \;\; \omega < \frac{1}{\sqrt{LC_2}}$$

$$Z_s \; is \; capactive \quad C = C_2 - \frac{1}{\omega^2 L} \quad When \;\; \omega \; > \frac{1}{\sqrt{LC_2}}$$

Equation 3-4

Therefore, $L_T$ can be expressed in terms of $C_1$, $C_2$ and L, as follows:

$$L_T = \frac{L}{1 - \omega^2 L C_2} - \frac{1}{\omega^2 C_1}$$

Equation 3-5

Based on Equation 3-5, the value of the fixed inductor can be selected as 2nH. The values of $L_T$ are selected based on the simulation results of section 3-1. The values of C1 and C2 can be calculated based on Equations 3-4 and 3-5.

The variable inductor circuit of Fig. 3-9 was incorporated into the previously developed ADS simulation bench to substitute the tunable inductor of the low pass Π network shown in Fig. 3-1. Fig. 3-10 presents the schematic of the proposed network.

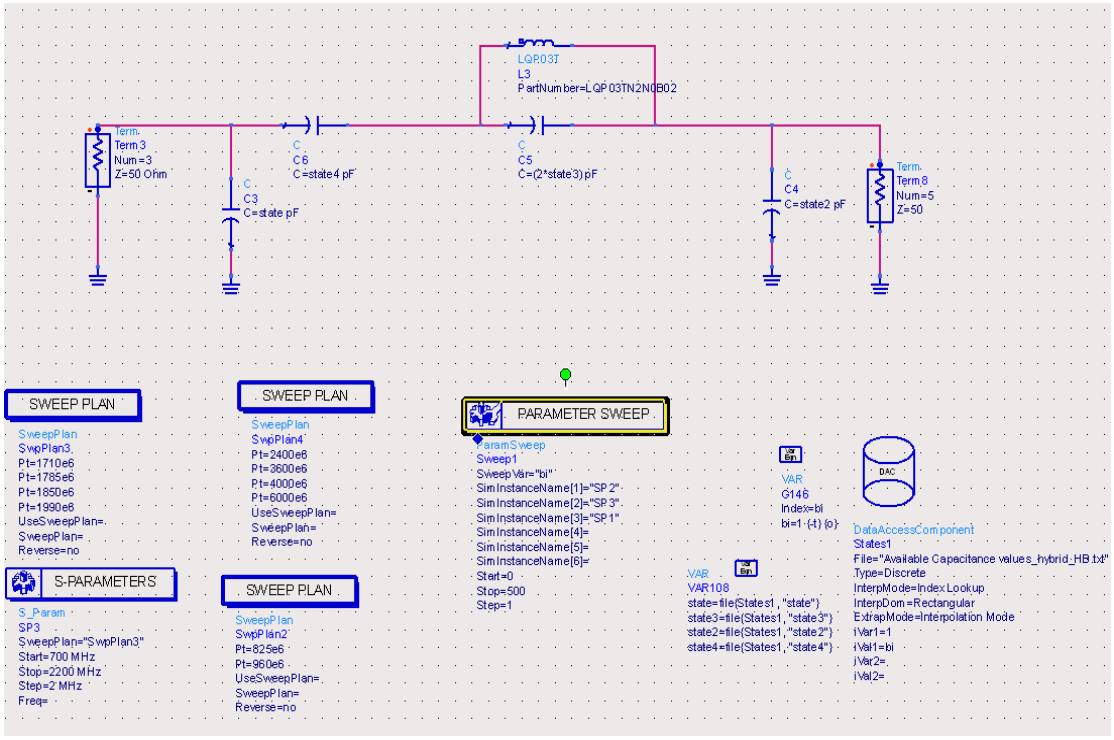


Figure 3-10: ADS simulation bench for tunable Π network based on fixed inductor.

We optimized the values of C1 and C2 in ADS, as follows. For the low band, we set C1 to 20 pF and spanned the variable capacitance $C_2$ from 1 to 10pF. For the high band, both C1 and C2 are variable capacitors with values spanned from 4 to 10 pF and 0.5 to 4 pF, respectively. For the series inductor in the schematic, we used a 2nH Murata inductor (part number LQP03TN2N0B02), incorporating the manufacturer published model of the inductor into the simulator [29]. Fig. 3-11 shows the tuning range for both low and high frequency bands.

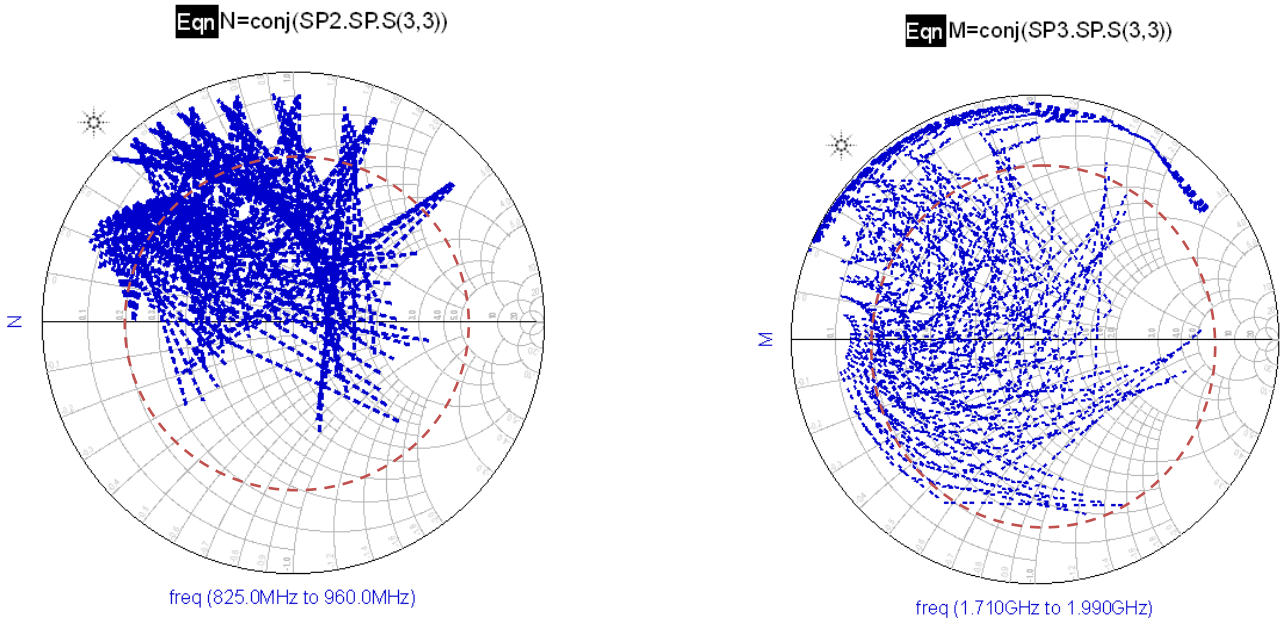


a) Low Band

b) High Band

Figure 3-11: Impedance dynamic range for hybrid impedance tuner.

From Fig. 3-11, we can observe that we can get good impedance coverage for the high frequency band within the 6:1 VSWR circle. However, for the low frequency band, the coverage is more offset toward inductive loads.

## 3.4 Characterization of Commercialized Tunable Element

Based on the previous simulation results and discussion, we use the low pass Π network to study the performance of tunable elements.

Several tuning techniques are discussed in [30] [31] [32], where variable capacitors based on MEMS, CMOS and BST are selected as tuning elements. In this section, we concentrate on BST-based capacitor tuning in a Π network configuration.

In [33], a BST circuit model was extracted from the quality factor, Q. Fig 3-12 illustrates a schematic of the BST circuit model [33].

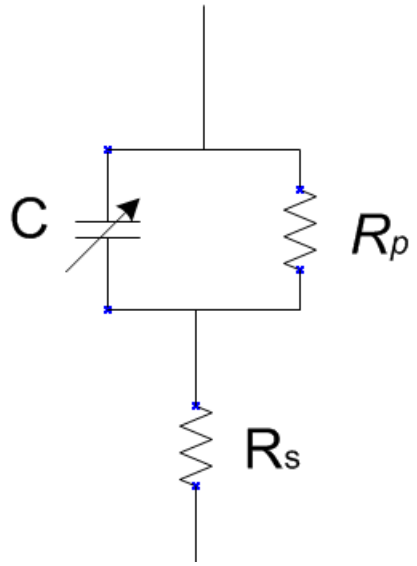


Figure 3-12: BST capacitor equivalent circuit model [33].

The quality factor of the BST capacitor is calculated using the following equations:

$$\frac{1}{Q_{total}} = \frac{1}{Q_{BST}} + \frac{1}{Q_{conductor}}$$

Equation 3-6

Where

$$Q_{BST} = \omega C R_p$$

Equation 3-7

$$Q_{conductor} = \frac{1}{\omega C R_s}$$

Equation 3-8

In order to extract the correct model for any BST capacitor, $R_s$ and $R_p$ must be known. However, in our example, $R_s$ and $R_p$ are unknown quantities. To quantify the $Q_{total}$ value of a BST capacitor, a commercially available part from On Semiconductor was characterized in a two-port network environment. The manufacturing part number of the BST used in the measurement is TCP-3047H. A datasheet of the part can be found in [34]. The bias voltage ranges from 2V to 20V, and the capacitance ranges from 4.7 pF to 1.24 pF. The maximum RF input power is 40 dBm.

We used two-port network analyzer to capture the scattering parameters (S parameters) of the BST capacitor. Fig. 3-13 shows the schematic of the developed test circuit. As can be seen, the RF1 and RF2 are both connected to the DC ground [34]. Murata RF ferrite beads were selected to be used as an RF choke. The main purpose of the RF choke is isolating the DC ground from the RF input and output pins of the BST.

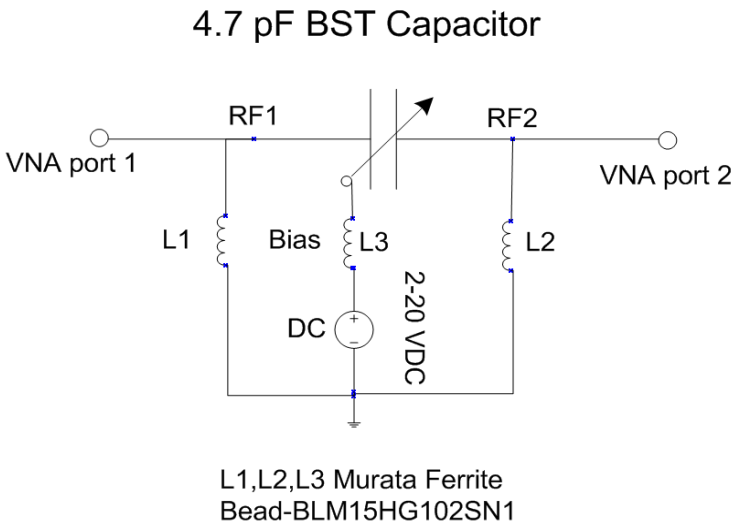


Figure 3-13: BST test circuit schematic.

We captured a set of S-parameter files when the bias voltage was swept from 2 to 20 volts. The scattering parameters are transformed to admittance parameter (Y-parameters) using the equations listed in [35], [36]. Fig. 3-14 presents the equations used in the ADS simulation bench to calculate the quality factor from the Y-parameters. Fig. 3-15 shows the calculated total quality factor based on admittance parameter.

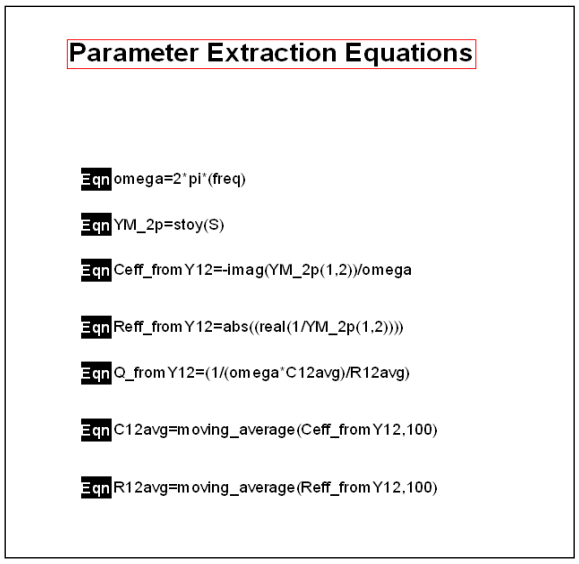


Figure 3-14: Q-factor calculations in ADS.

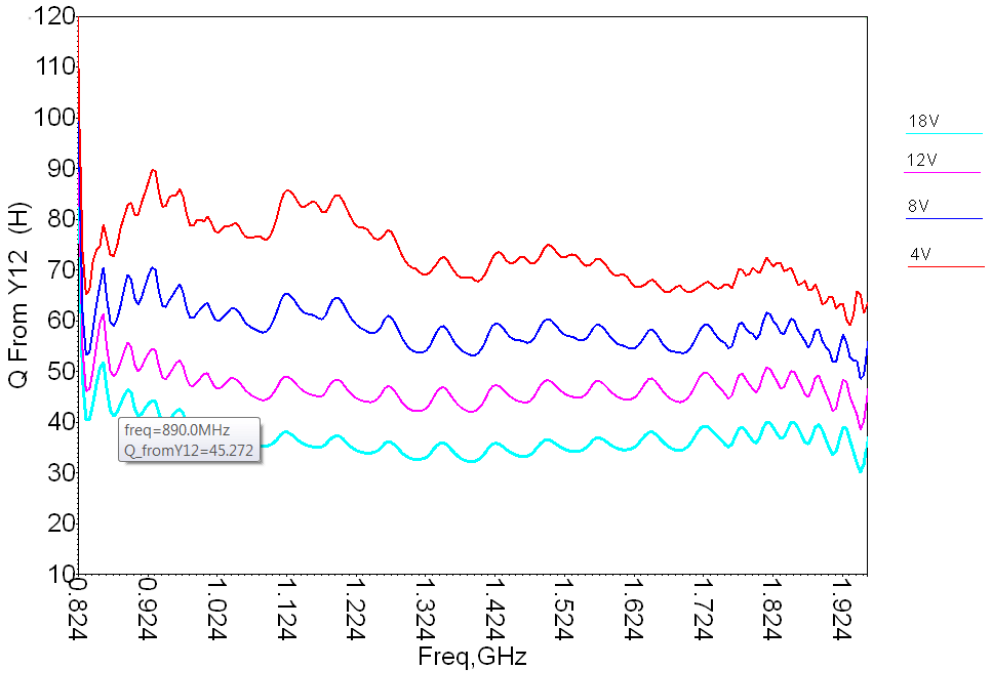


Figure 3-15: Quality factor for On Semiconductor 4.7pF BST capacitor.

Fig. 3-16 shows the effective resistance and effective capacitance of the BST capacitor. These values are also used in Chapter 4 of this thesis to build accurate model of the tuning elements in the simulator.

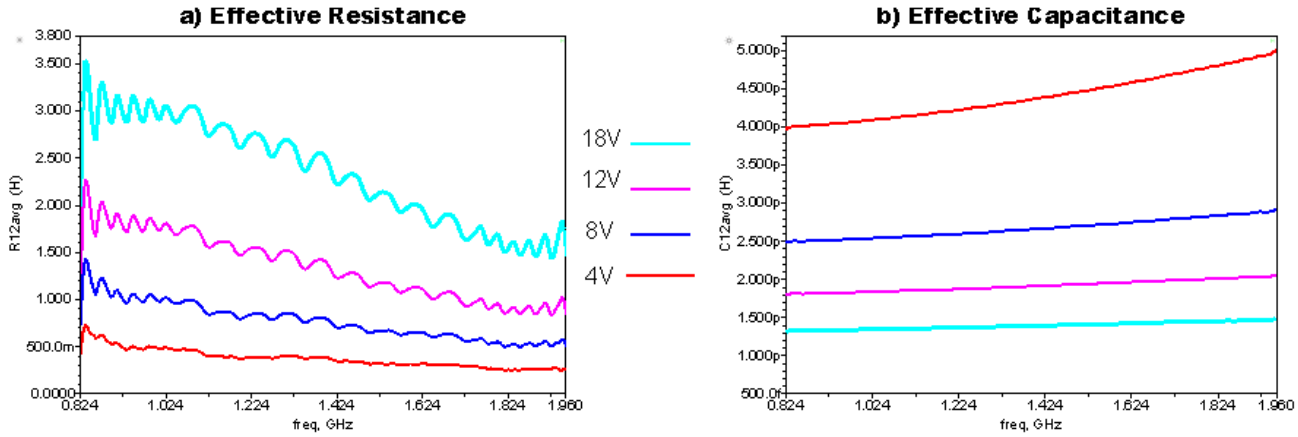


Figure 3-16: Effective resistance and effective capacitance of 4.7 pF BST at different bias voltages.

From Fig. 3-15 and Fig. 3-16, we can deduce that the BST capacitor under evaluation suffers high losses when the bias voltage increases to cover wide tuning range. This reflects on high values of the effective resistance of the BST capacitor, and hence the quality factor is reduced significantly.

To illustrate the poor quality factor of the BST tunable capacitor, we conducted a simulation on a ceramic capacitor with the same capacitance. Fig. 3-18 shows the quality factor for a 1.3pF ceramic capacitor offered by Murata Manufacturing [37]. The quality factor of the part at 1990 MHz is 247, which is significantly larger when compared to the quality factor of the BST.

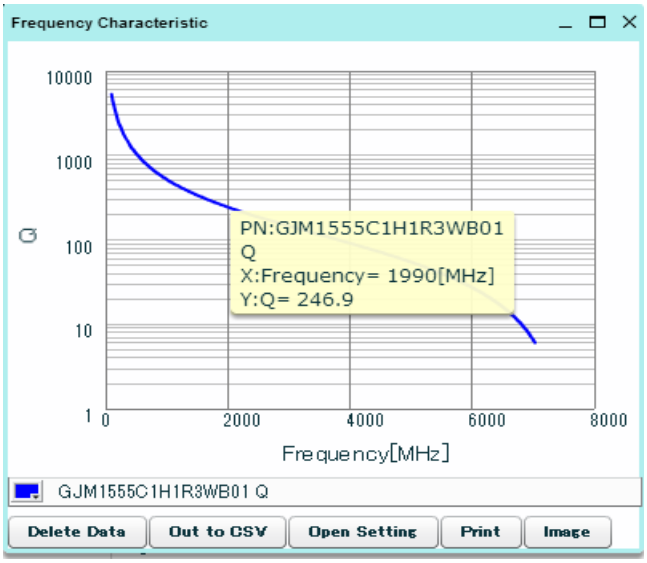


Figure 3-17: Quality factor of fixed 1.3 pF ceramic capacitor.

The measured S-parameter files were used to build a multi-dimensional two-port s-parameter file (S2PMDIF). The S2PMDIF file is plugged into the ADS simulation bench to capture the tuning range of the low pass Π network.

Fig. 3-17 shows a schematic of the BST-based low pass Π tuning network we developed. Fixed value inductor models are used [29] for each frequency band.

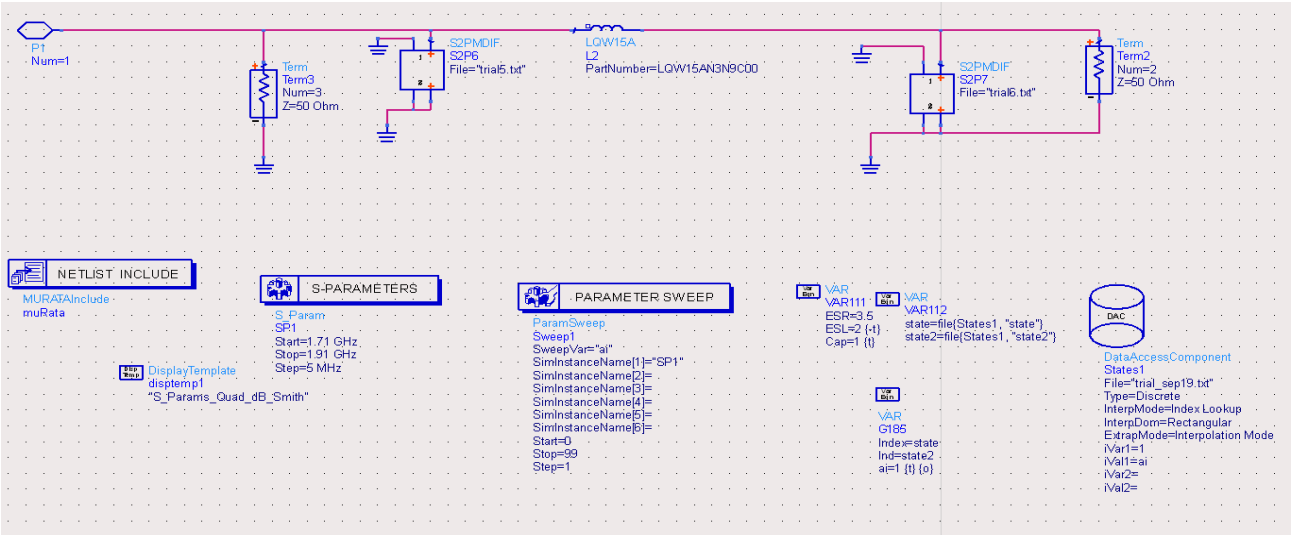


Figure 3-18: BST based low pass Π tuning network.

Fig. 3-18 illustrates the tuning range and insertion loss of the network at the low and high frequency bands, respectively. It can be seen that the insertion loss is high at certain bias conditions. Designers can avoid these high loss points, which will reduce the tuning dynamic range of the network.

It can be also concluded that the series inductor value can shift the impedance coverage to any desired location on the Smith chart. This can be optimized in the design based on prior knowledge with the antenna impedance.

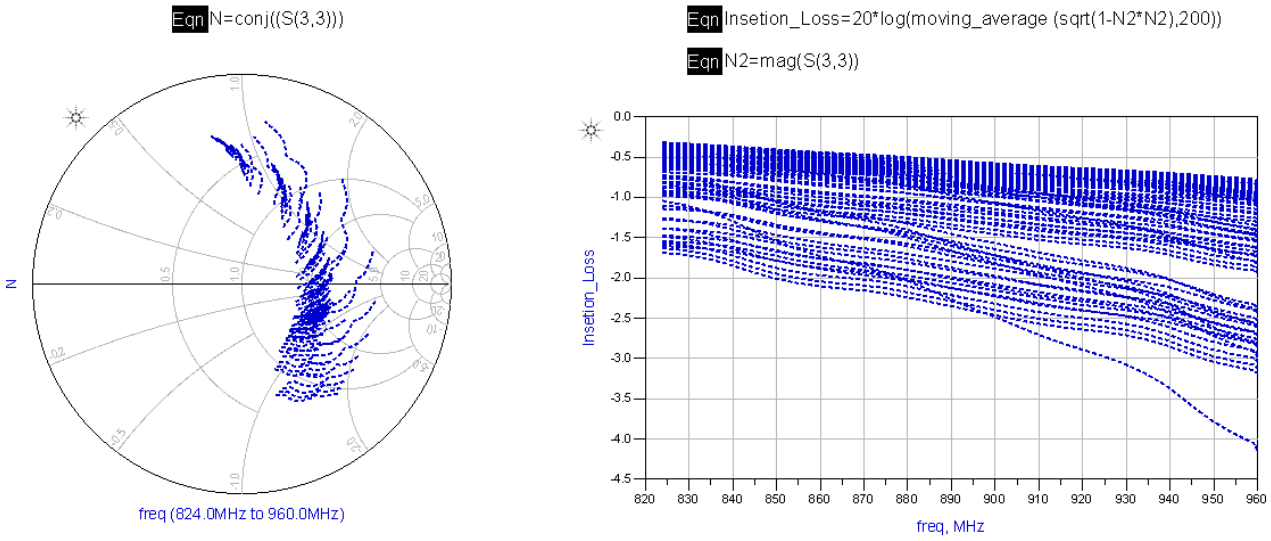


a) Low Band

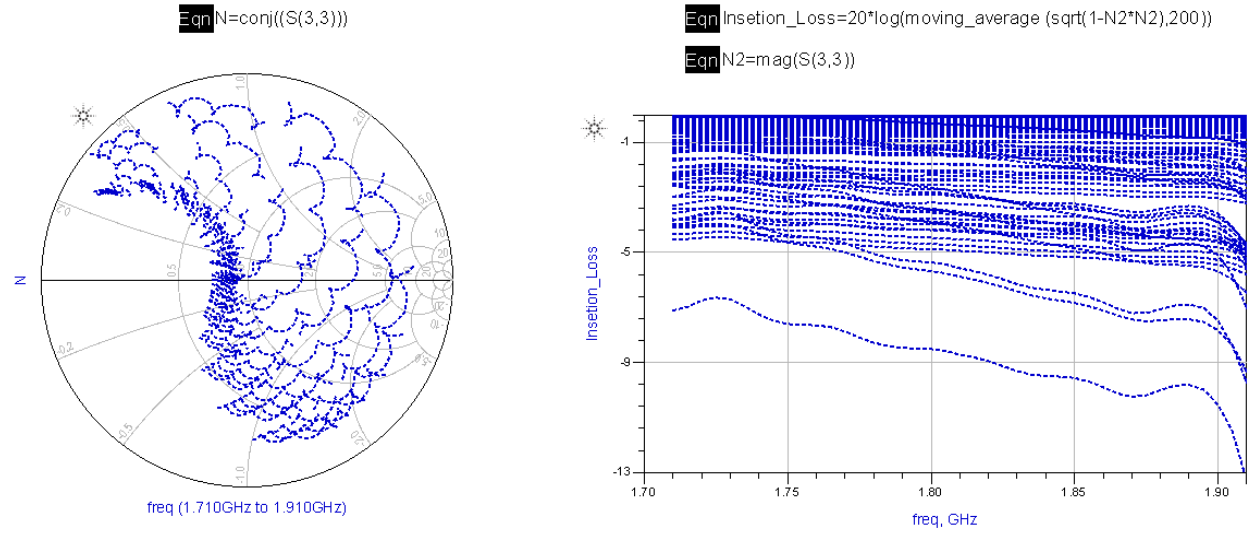


b) High Band

Figure 3-19: Tuning range and insertion loss of BST-based Network: a) Low Band; b) High Band.

## 3.5 Conclusion

The simulation results for multiple impedance tuning networks demonstrated the impedance dynamic range of each network. The results showed that low pass Π networks can be the ideal topology candidate for adaptive impedance tuners.

Low pass Π networks can provide the following desired criteria:

a) Wider impedance tuning dynamic range within the bench mark VSWR range.

b) Single inductor utilization.

We also demonstrated a technique for substituting variable inductors with a fixed inductor and two variable capacitors.

We studied the performance of an off-the-shelf BST capacitor and characterized the following physical quantities:

a) Quality factor at different bias points.

b) Effective resistance and effective capacitance at different bias points.

The calculated effective resistances were significant at certain bias point. This caused degradation of the quality factor at these points.

The BST captured models were used in ADS simulation to study the performance. A 99-state impedance tuning network was simulated, and the results showed the ability of the network to cover a wide range of load impedance. However, the insertion losses were significant at certain states. These states should be avoided in the practical implementation of such a network.

# Chapter 4
# Aperture Tuning

In this chapter, we perform a detailed study to compare tunable matching networks and tunable antenna elements. The study is mainly focused on ascertaining which method will help achieve the design targets in terms of system capabilities for transmitting and receiving RF power.

The antenna design used for this study is a practical design used in a machine-to-machine communication (M2M) device. The M2M device is designed by a Waterloo, Ontario, technology company (DBJay Technologies LTD), model number ZJ100 [38]. The device used in this study comprises a quad band GSM radio design, GPS radio, and ISM radio. Although three antennas are used in this radio, we focus on the GSM antenna. The antenna was designed to cover only the 900 MHz and 1800 MHz bands.

The covered bands are used in Europe and China [39]. In order for this device to work in North America, the antenna resonance had to be shifted to cover the 850 MHz and 1900 MHz bands. In practice, this can be done by changing the design and physical length of the antenna element. However, we show here how such physical design changes can be avoided.

The following study is our contribution of how the above technical problem can be solved using two different methods, as follows:

a) using a tunable antenna element or aperture tuning; and
b) using a tunable matching network.

The methodology we developed is as follows:

a) Construct an accurate model for the current antenna design in an Ansoft High Frequency Structure Simulator (HFSS) [40].
b) Obtain surface current distribution from the simulation results to determine the most suitable location for inserting tuning elements [14].
c) Sweep the value of the tuning elements and capture S11 and field strength in each case.
d) Simulate the performance using a tunable matching network and compare the results to the aperture tuning method.
e) Capture baseline measurement for radiated RF power using the actual hardware. All measurements are executed using Dart 3300E RF anechoic chamber from Tri L Solutions [41].
f) Modify the physical device antenna by inserting different tuning elements. Capture radiated RF power measurements for each case.
g) Design a tunable matching network using the techniques discussed in Chapter 3. Capture the radiated power for each mode of the tuning network.
h) Compare the results.

## 4.1 Tunable Antenna Element

The design methodology of a tunable antenna was presented in [14]. The design model was built in an Ansoft High Frequency Structure Simulator (HFSS) [40]. The model shown in Fig.4-1 was built to match the exact dimensions and materials of the practical design. Specific attention was paid to modeling the RF components used for matching networks or for tuning.

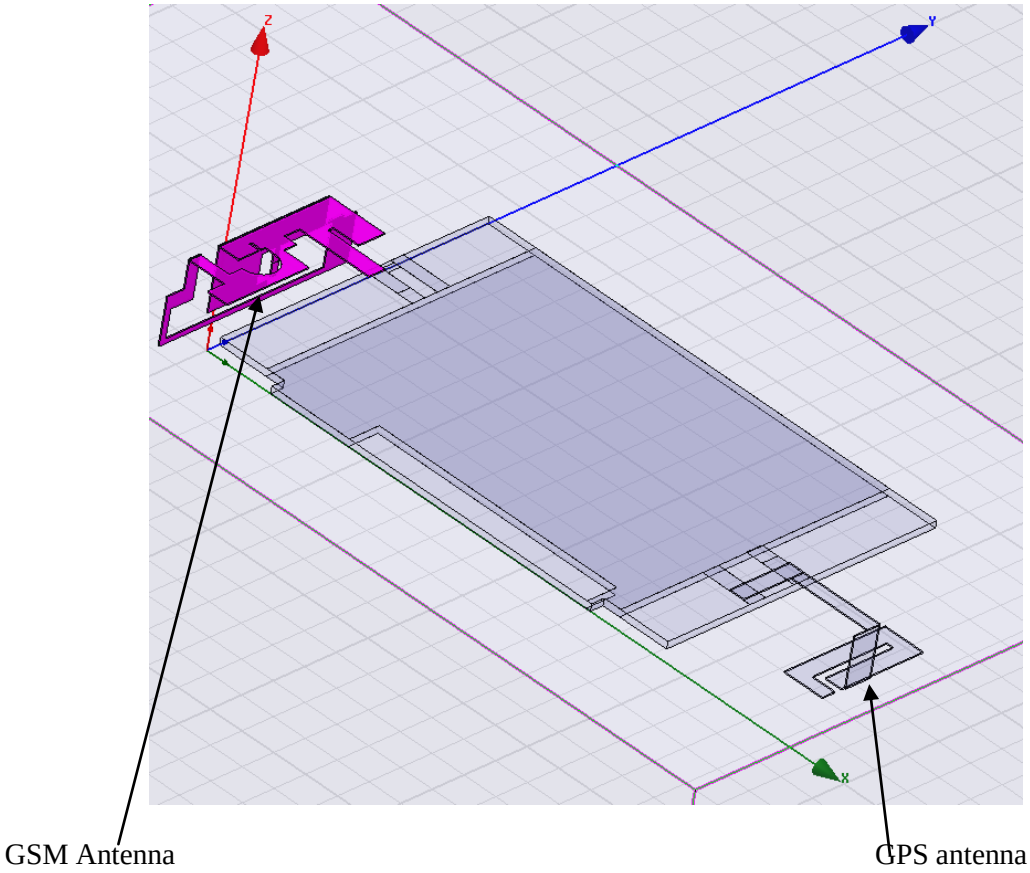


Figure 4-1: M2M device model built in HFSS simulator.

### 4.1.1 Lumped RF Components Modeling

The original antenna matching network comprises a single inductor manufactured by Murata Inc. The part number of the inductor is LQP03TN6N8H02. The nominal value of the inductor is 6.8nH. For accurate results, the original matching circuit was modeled using the component Web-Based simulation tools from Murata [37].

For the selected package, the effective resistance is 1 ohm for frequencies up to 1 GHz and 2 ohms for frequencies up to 2 GHz. The equivalent inductance of the package is slightly larger at higher frequencies. The parasitic capacitance is calculated using Equation 4-1. The self-resonance frequency is found in the component datasheet [42].

Fig.4-2 shows the Murata film inductor equivalent circuit. Table 4-1 summarizes the values used for the simulation at discrete frequency points that match the middle channel frequencies for the four GSM frequency bands.

$$F_{SR} = \frac{1}{2\pi\sqrt{L_{eq}C_p}}$$

Equation 4-1

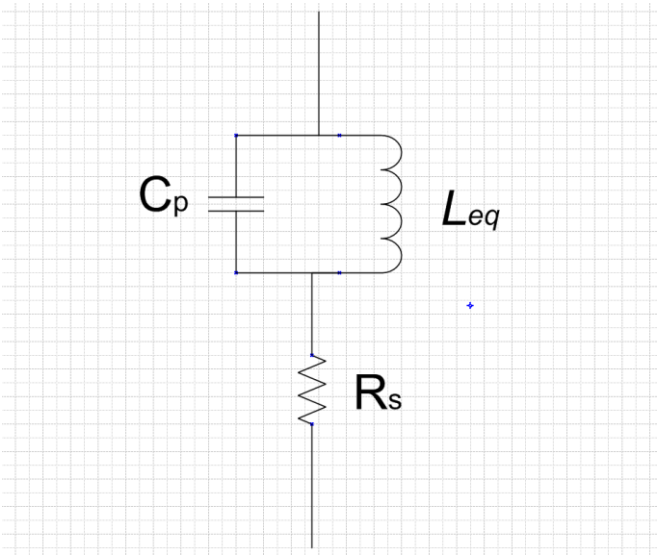


Figure 4-2: Murata film inductor equivalent circuit.

Table 4-1: Equivalent values used for simulation.

| Frequency | Rs (ohm) | L (nH) | Cp (pF) |
|---|---|---|---|
| 836 MHz | 1 | 6.8 | 0.13 |
| 897 MHz | 1 | 6.8 | 0.13 |
| 1747 MHz | 2 | 7.2 | 0.13 |
| 1880 MHz | 2 | 7.3 | 0.13 |

### 4.1.2 Baseline Simulation Results

We used the HFSS full wave simulator to determine the base line simulation results for the antenna element. Fig. 4-3 shows the antenna S11 in dB scale. As can be seen, the antenna is well tuned at the GSM1800 MHz and GSM1900 bands and poorly tuned at the GSM900 MHz band. We also note a mismatch at the GSM850 MHz band.

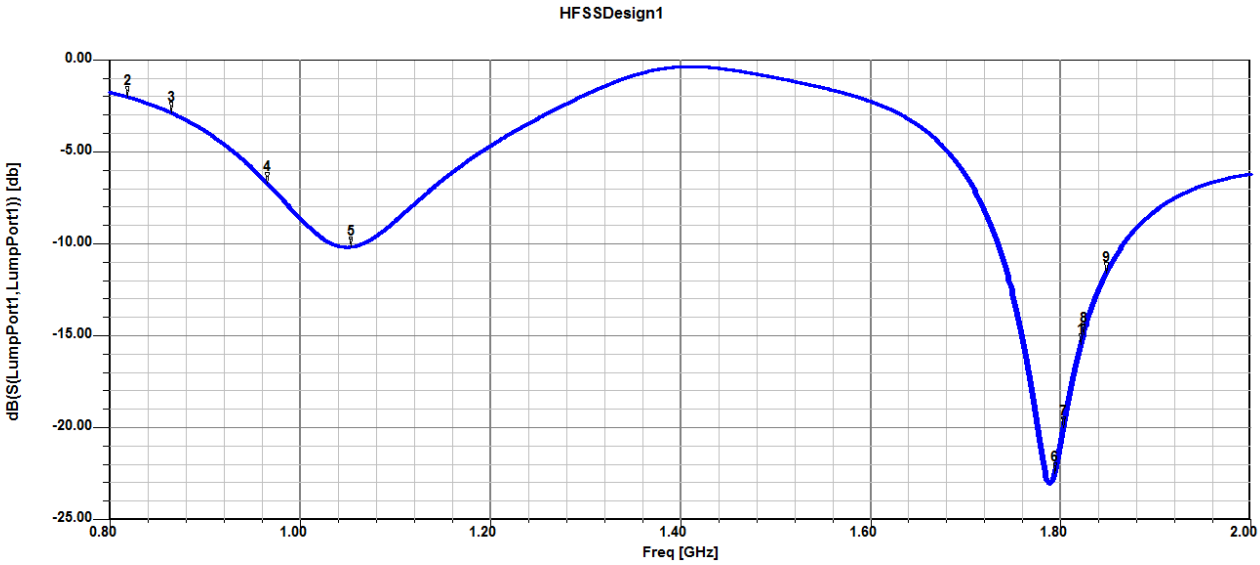


Figure 4-3: Antenna baseline S11 simulation results.

In order to obtain complete baseline simulation results, we must consider the radiated power of the antenna along with the radiation pattern. Fig. 4-4 and Fig. 4-5 illustrate the baseline radiated fields at the middle channels of the four GSM bands.

As can be seen in Fig. 4-4 and Fig. 4-5, the radiated fields reflect the matching condition of the antenna. For GSM850, the peak radiated field is 13 dB. As the matching improves, the radiated fields become stronger. The peak field strength occurs in the GSM1800 band and reaches more than 20dB.

+

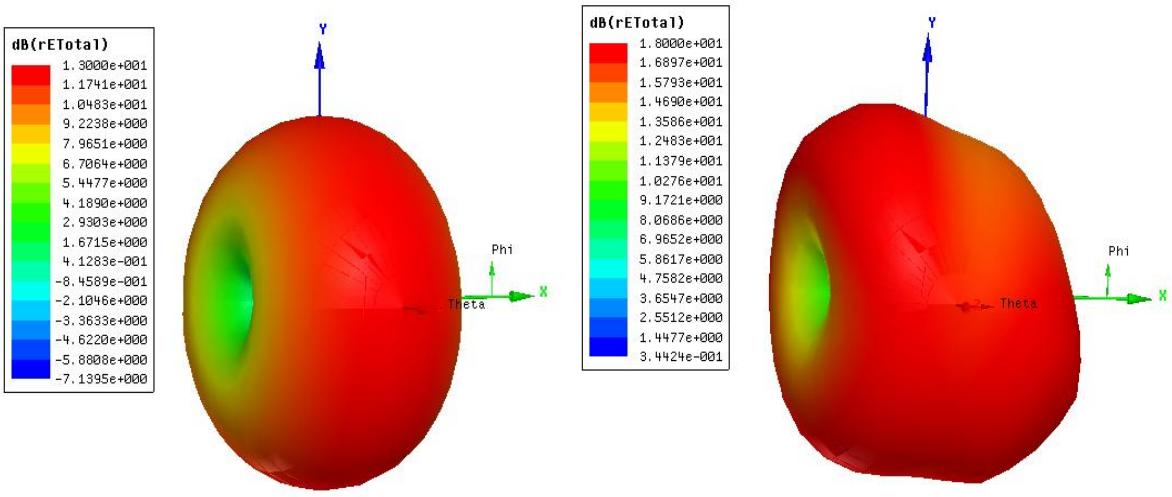


a) GSM850 b) GSM1900

Figure 4-4: Baseline-simulated total radiated field: a) GSM850; b) GSM1900.

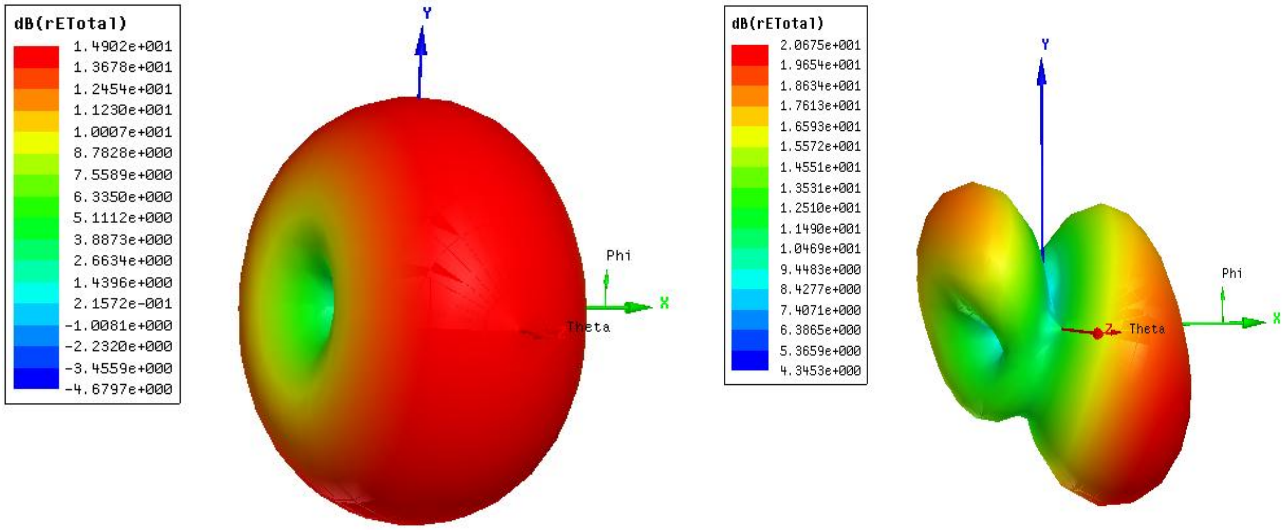


a) GSM900 b) GSM1800

Figure 4-5: Baseline-simulated total radiated field: a) GSM900; b) GSM1800.

The surface current characteristics determines the radiation pattern and efficiency of an antenna, thus, they are of specific interest. The effectiveness of the tuning elements is highly dependent on surface current distribution [14] [26]. In low current points, the voltage is maximum, and so a series-tuning element will not be effective. Using circuit analogy, the minimum current points can be considered as open circuit; hence, any series-lumped element will have minimum impact on the antenna characteristics. Similarly, in maximum current points, the voltage is minimum. Therefore, loading the antenna aperture with a shunt tuning element will greatly reduce the effective aperture size, resulting in reduced efficiency and bandwidth.

On the other hand, adding a tuning element at a high current area can cause an effect equal to extending the physical length of the antenna or pulling the resonance to lower frequencies. Fig. 4-6 and Fig. 4-7 show the surface current distribution for the four GSM bands.

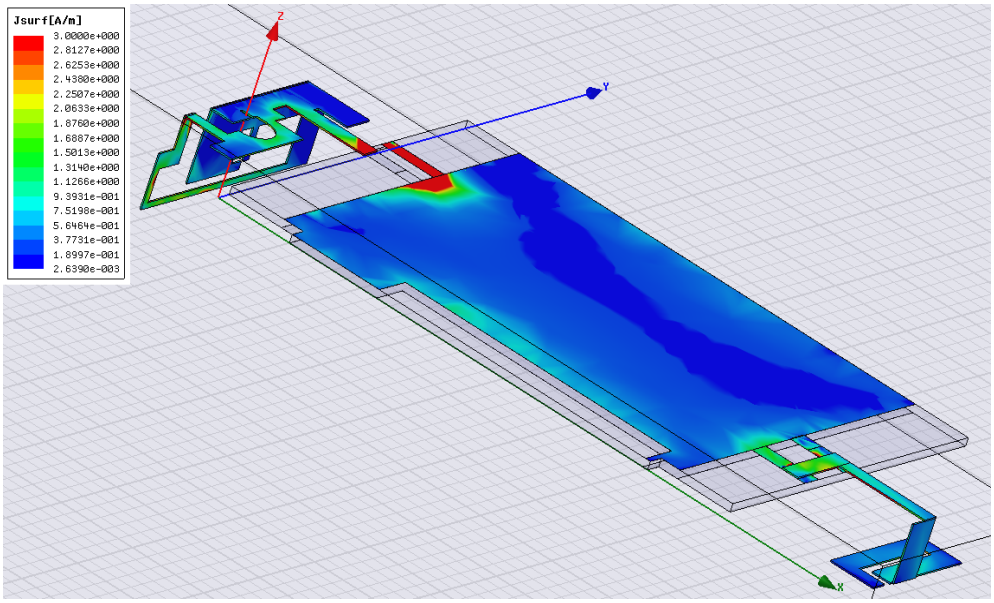


a) GSM850

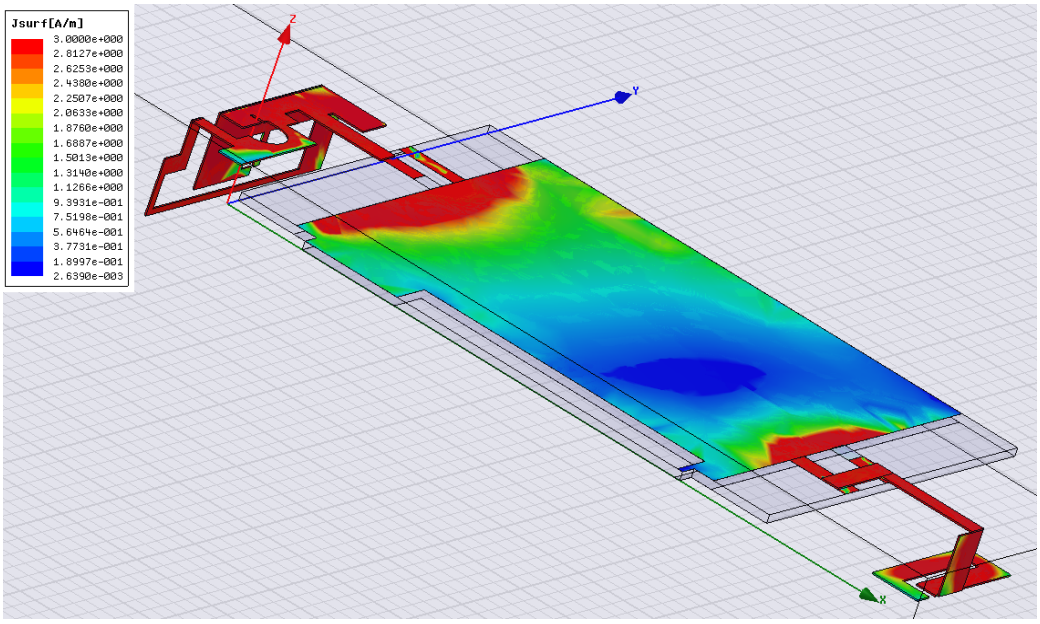


b) GSM1900

Figure 4-6: Surface current distribution: a) GSM850; b) GSM1900.

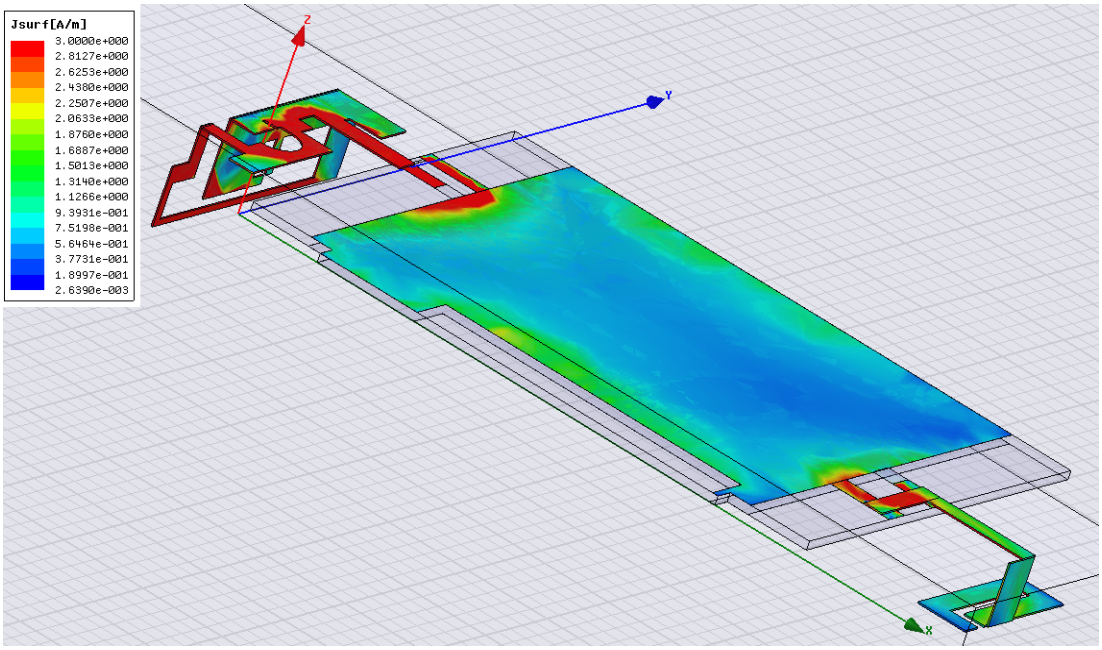


a) GSM900

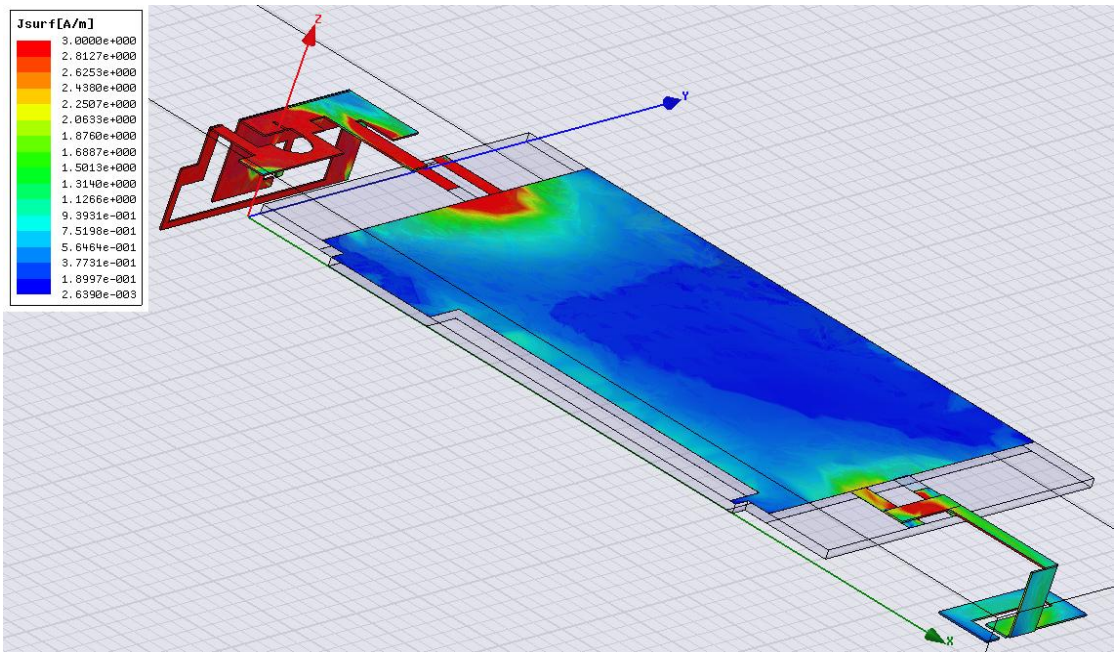


b) GSM1800

Figure 4-7: Surface current distribution: a) GSM900; b) GSM1800.

From Fig. 4-6(a), we can deduce that the RF current fed from the port is not being accepted by the antenna element. For the GSM850 band, the strong currents are localized at the antenna feed, and thus it does not cause efficient radiation. From Fig. 4-6(b), we can observe higher current flow and better radiation. From Figs. 4-7 (a) and (b), we can observe large current flow on the antenna element, resulting in enhanced radiation. We can also locate the maximum current points on the antenna element for each band to find the optimum location for inserting tuning elements.

### 4.1.3 Series Elements-Based Aperture Tuning

Based on the previous discussion, we start by adding lumped RF component (inductor or capacitor). The component is then inserted in series at high current points.

The values of the tuning elements are swept until the optimum performance is found. Fig. 4-8 shows the selected location of the series element. This is driven by the maximum surface current amplitude.

The study was done in two steps:

- series inductor-based tuning; and
- series capacitor-based tuning.

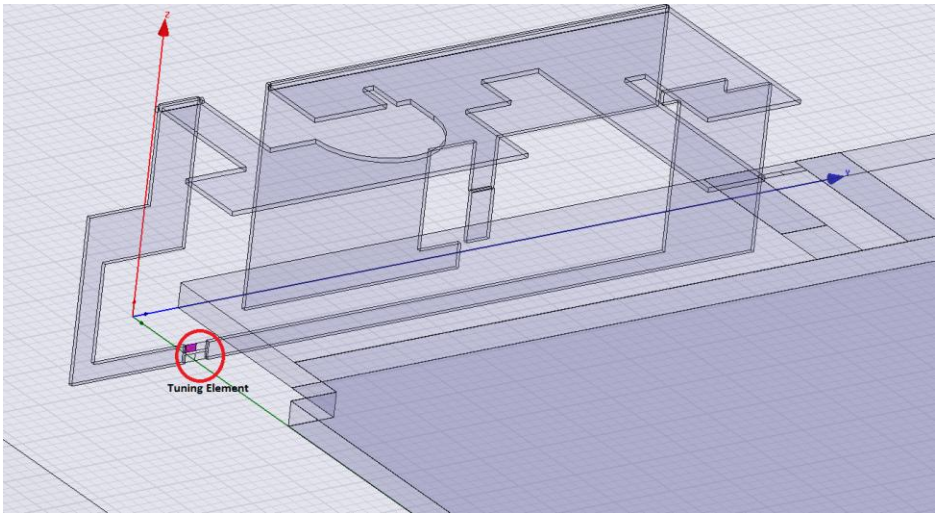


Figure 4-8: Location of tuning elements.

### 4.1.3.1 Series Inductor-Based Aperture Tuning

We used Murata RF inductors LQW series [42] for the first part of this study. We extracted the correct inductor model using the technique described in section 4.1.1. and conducted several simulation runs to experimentally select inductor values. The values selected were 20, 15, 10, and 5 nH.

Figs. 4-9, 4-10, 4-11 and 4-12 show the total radiated field for each of the selected inductor values. From Fig.4-9, we observe a maximum increase of 1.7 dB in the radiated field of the GSM850 when 20 nH inductor was used, which is aligned with the maximum improvement of the antenna return loss at this frequency. From Fig. 4-10, we observe a maximum increase of 1.7 dB in the radiated field of the GSM900 when a 15nH inductor was used, which is aligned with the maximum improvement of the antenna return loss at this frequency. From Fig. 4-11 and Fig. 4-12, we observe minimum variations from the baseline results; hence, the effectiveness of the inductors is minimal.

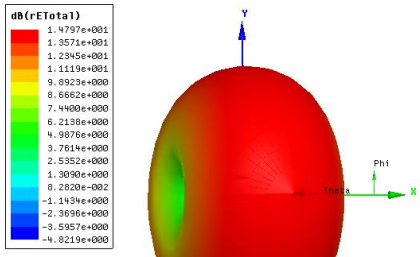


a) GSM850

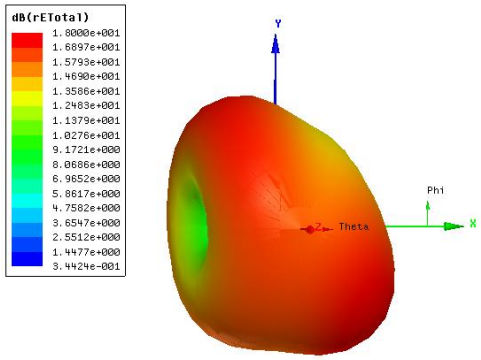


b) GSM1900

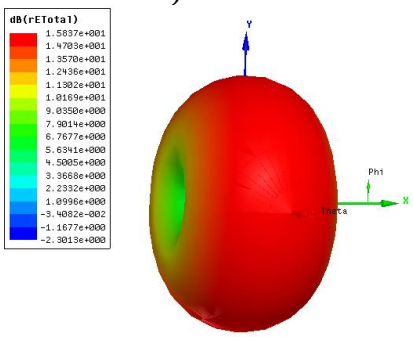


c) GSM900

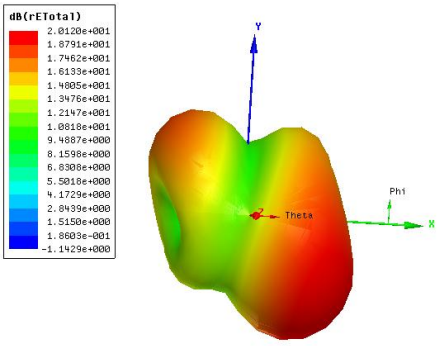


d) GSM1800

Figure 4-9: Radiated fields – Inductor value 20 nH.

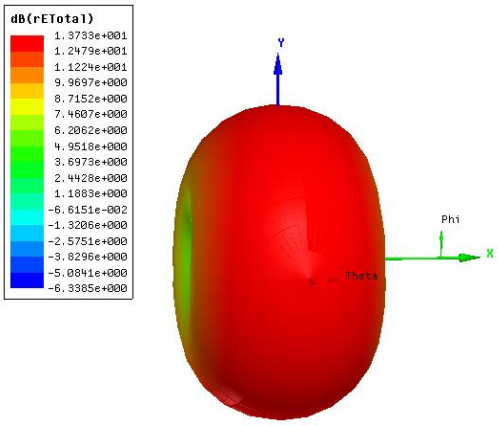


a) GSM850

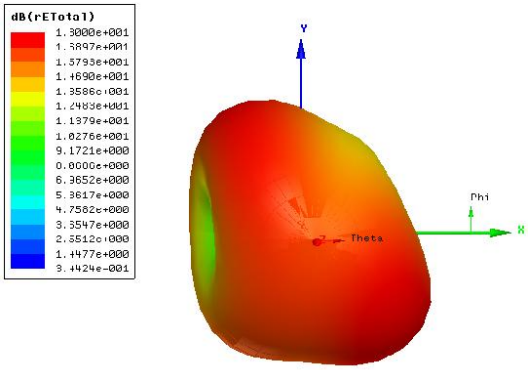


b) GSM1900

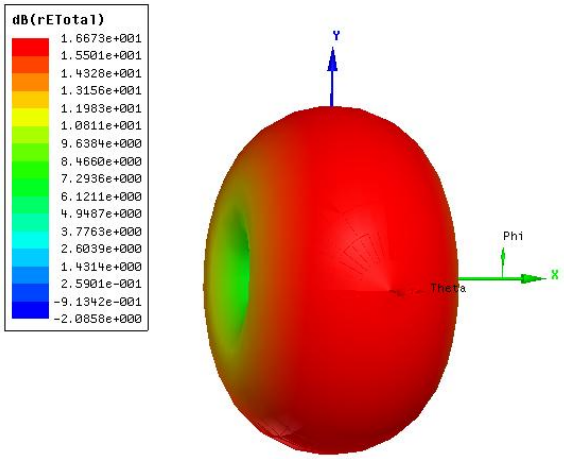


c) GSM900

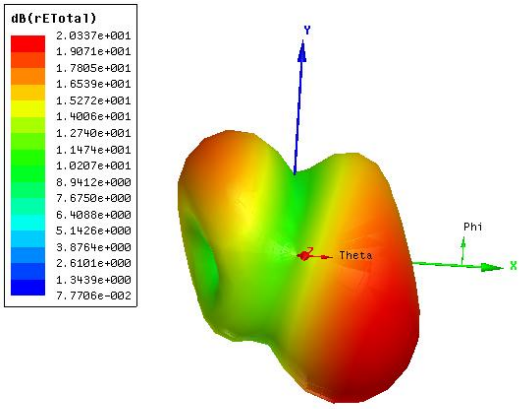


d) GSM1800

Figure 4-10: Radiated fields – Inductor value 15 nH.

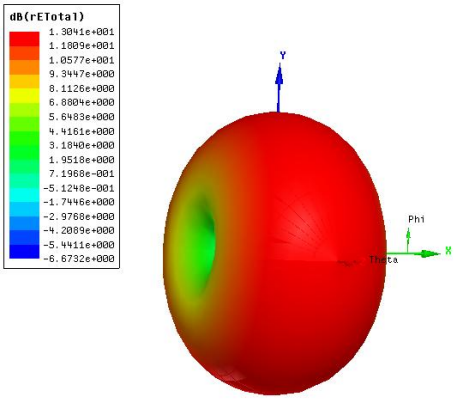


a) GSM850

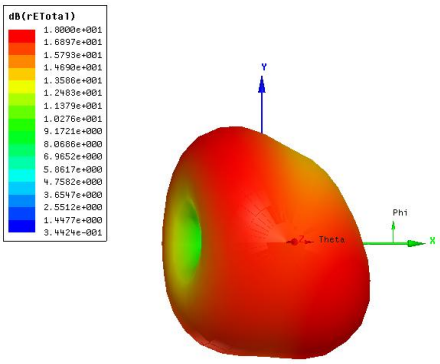


b) GSM1900

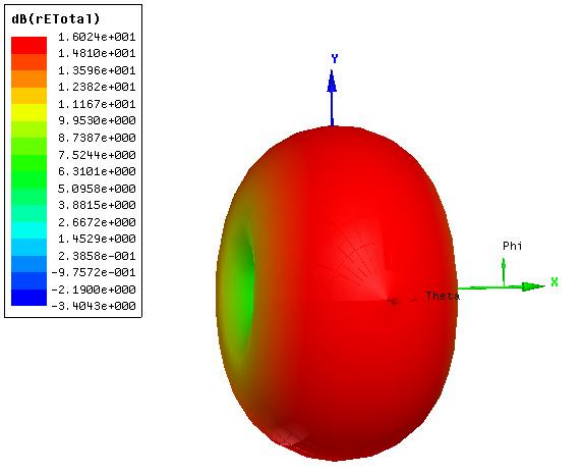


c) GSM900

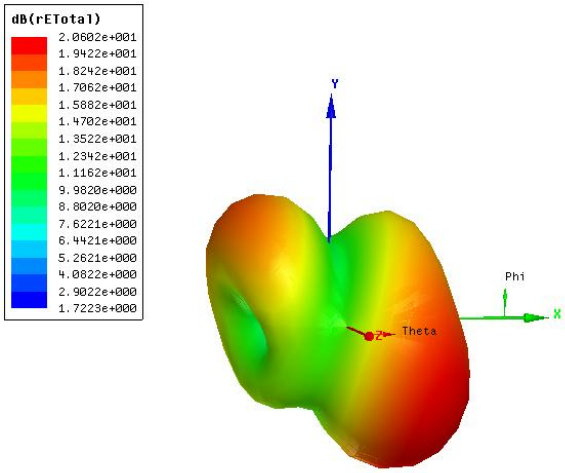


d) GSM1800

Figure 4-11 Radiated fields - Inductor value 10 nH

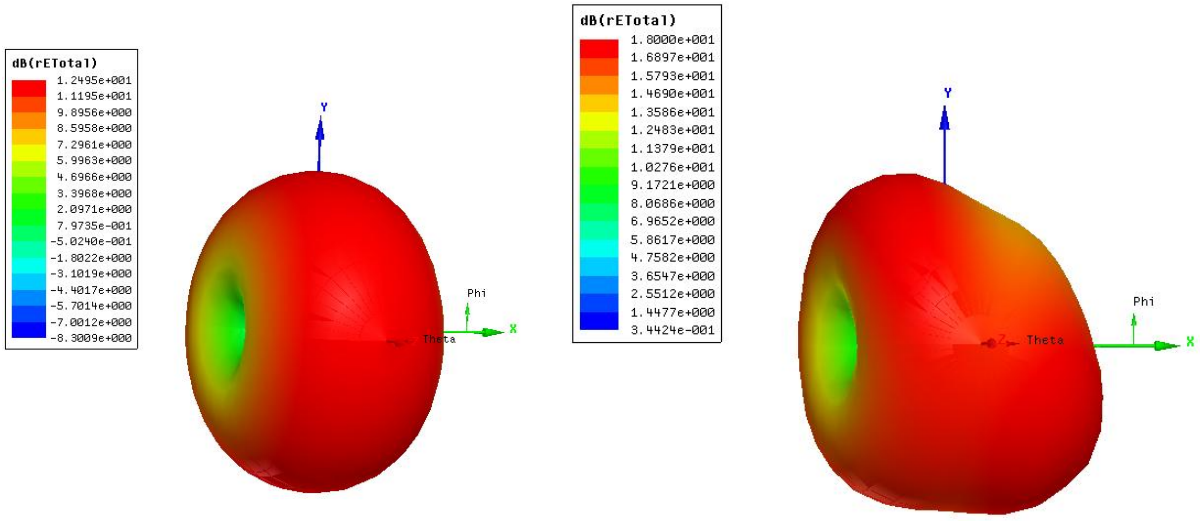


a) GSM850 b) GSM1900

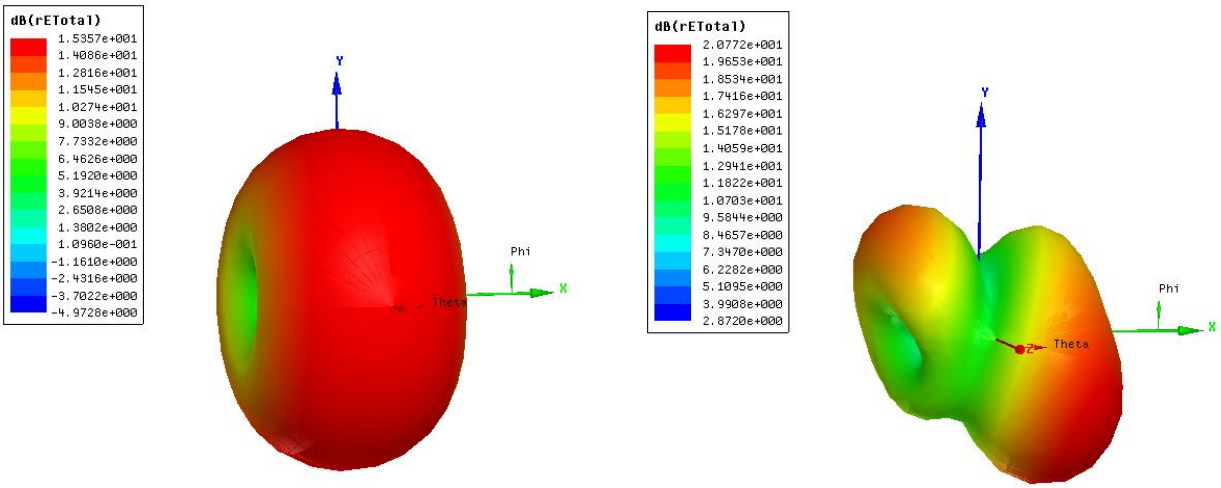


c) GSM 900 d) GSM1800

Figure 4-12: Radiated fields – Inductor value 5 nH.

Also from Fig.4-9 and Fig.4-10, we observe 0.7dB degradation in the GSM 1800 peak radiated field when 20nH and 15nH inductors are used. However, from Fig.4-12, we observe a 0.2dB increase when 5 nH inductor is used.

As for the GSM1900, there is no significant change in the peak radiated field. However, the radiation pattern changed to reflect lower radiation in some directions, as shown in Fig. 4-13.

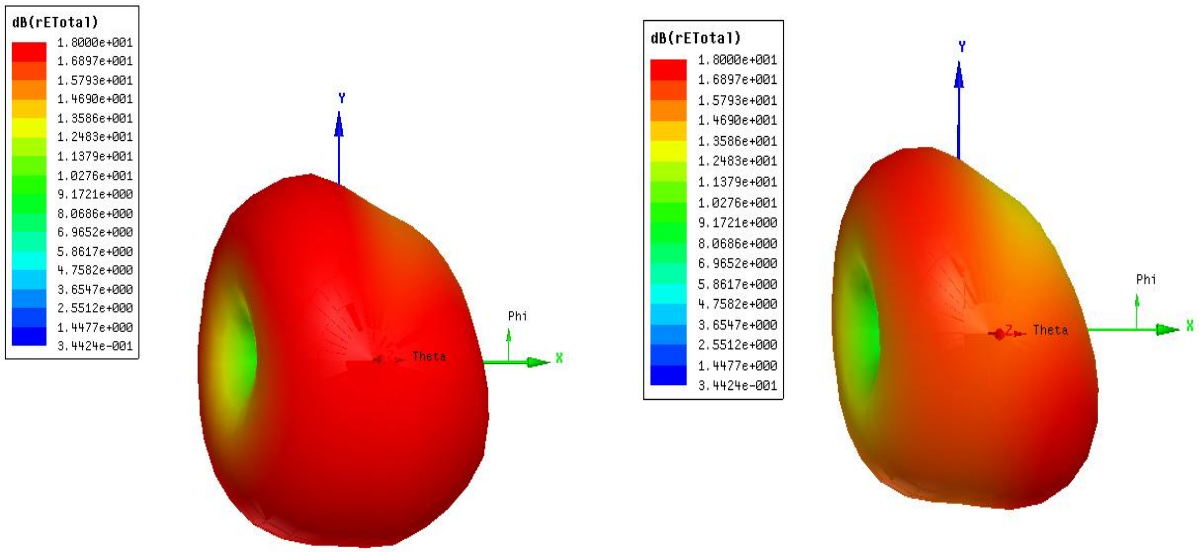


a) Baseline radiated fields GSM1900 b) 20nH radiated fields GSM1900

Figure 4-13: Radiated fields comparison for GSM1900.

## 4.1.3.2 Series Capacitor-Based Aperture Tuning

We used Murata RF GRM series capacitors for the second part of this study [37]. The correct capacitor model was extracted using the technique described in section 4.1.1. We conducted several simulation runs to experimentally select capacitor values. The values selected to conduct

the study are 5 and 2pF. Figs. 4-14 and 4-15 show the total radiated power for each of the selected capacitor values.

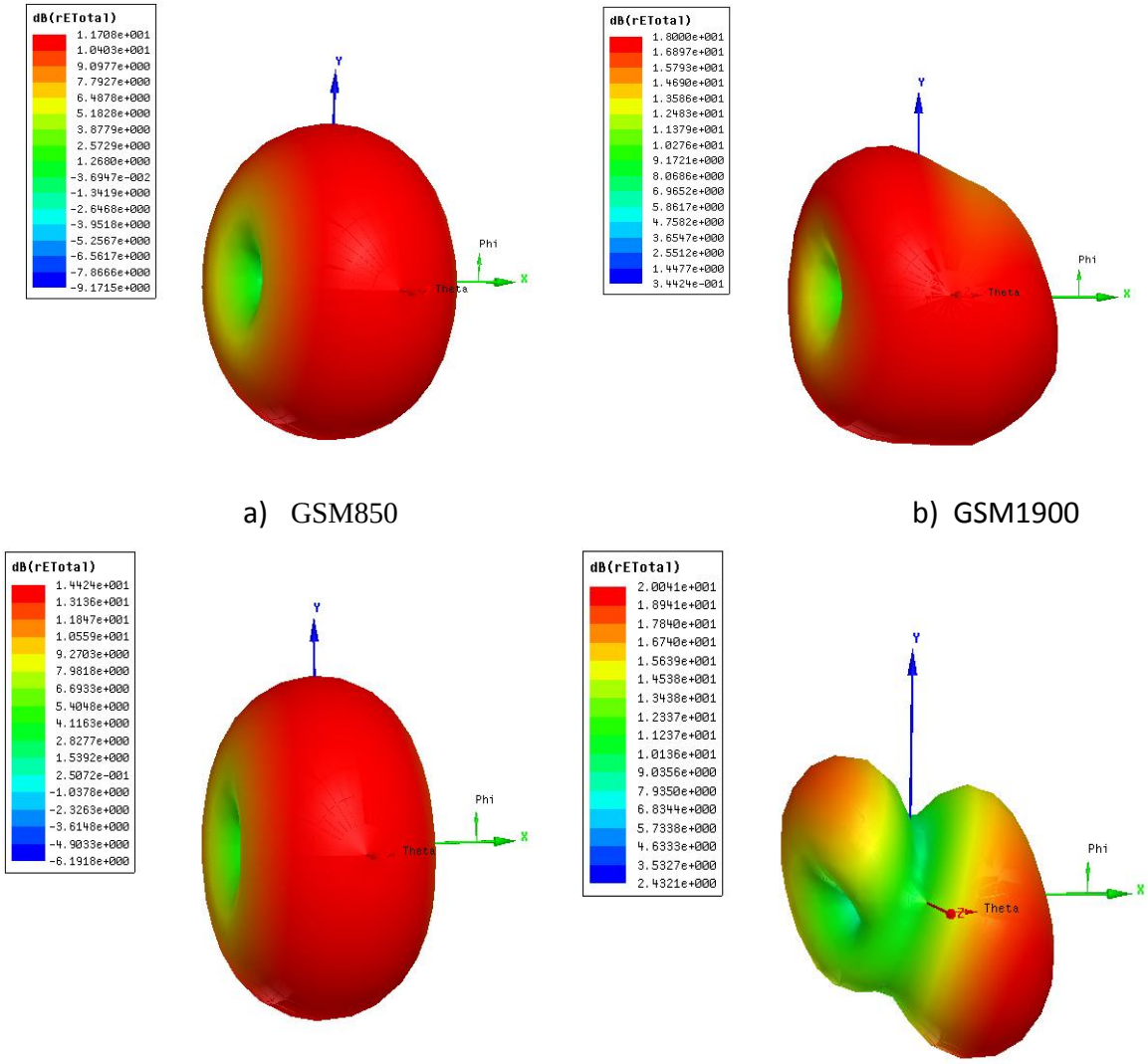


a) GSM850 b) GSM1900

c) GSM900 d) GSM1800

Figure 4-14: Radiated Power – Capacitor value 5pF.

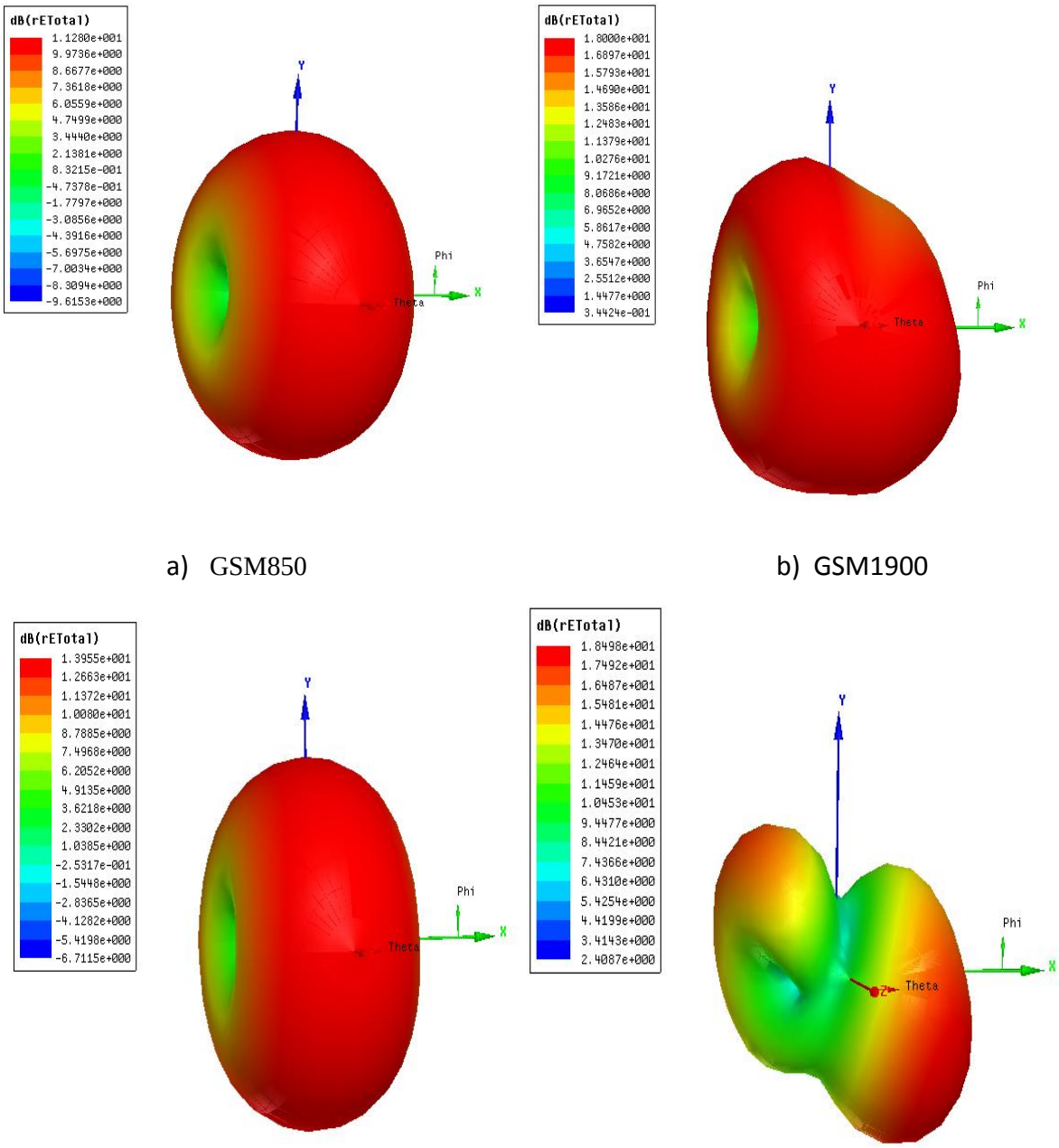


a) GSM850

b) GSM1900

c) GSM900

d) GSM1800

Figure 4-15: Radiated Power – Capacitor value 2pF.

From Fig. 4-13 and Fig. 4-14, we observed a 0.2 and 0.1dB degradation in the radiated field for the GSM850 and GSM900, respectively. For the GSM1800 band, we observed a degradation of 0.6dB when the 5pF capacitor was used and a degradation of 1.9dB when the 2pF capacitor was used. For the GSM1900 band, we observed no change in the peak radiated fields.

## 4.2 Tunable Matching Network

The initial work performed in finding the matching network was done using Smith v3.0 simulation software [43] and Agilent Advanced Design System [36]. Discrete frequency points were entered into the simulator to deduce the matching network, which was then incorporated into the HFSS full wave simulator [40]. The modeling of the lumped elements was done using the same technique described in section 4.1.1.

The location of the matching network is shown in Fig. 4-16, and the schematic of the matching network is shown in Fig. 4-17.

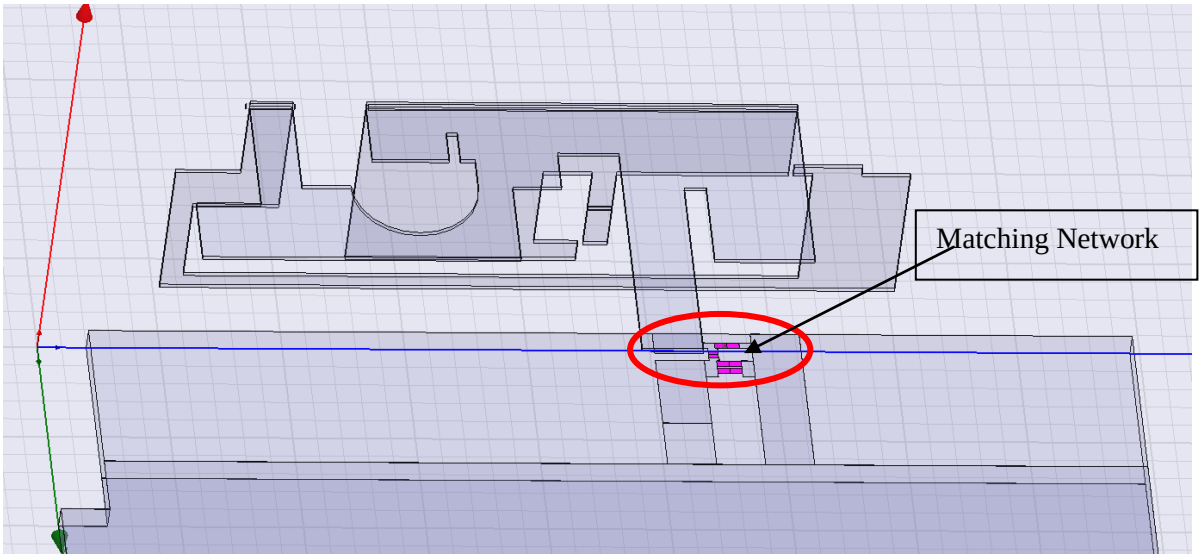


Figure 4-16: Location of the matching network.

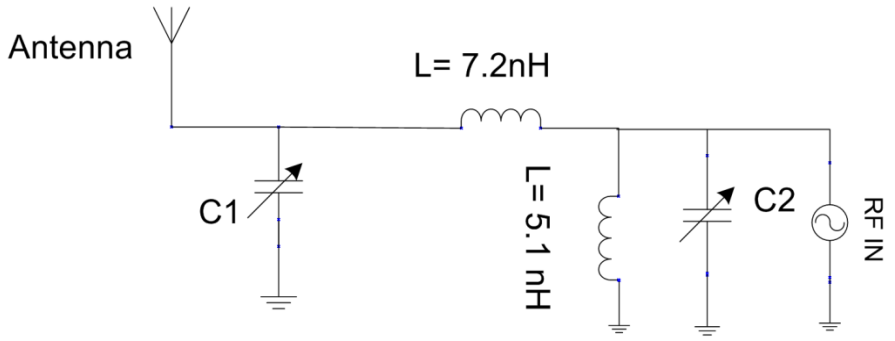


Figure 4-17: Schematic of the matching network.

It can be deduced from the schematic in Fig. 4-17 that the impedance can be tuned by changing the capacitors values in the circuit. This is favored over changing the inductor value, as such components are not yet widely available.

The tuning strategy is based on finding the optimum values for the capacitors to cover each individual band. Performance measures such as total radiated power and input return loss are evaluated for each band. Table 4-4 shows the values of capacitors C1 and C2 for each frequency band. The used capacitor model is extracted from the measurement results presented in section 3.3.

Table 4-2: Capacitor values for each frequency band.

| Frequency | $C_1$ (pF) | $R_{eff1}$ (ohms) | $C_2$ (pF) | $R_{eff2}$ (Ohms) |
|---|---|---|---|---|
| 836 MHz | 1.3 | 2 | 1.3 | 2 |
| 897 MHz | 0.5 | 2 | 5 | 0.5 |
| 1747 MHz | 1 | 2 | 2.7 | 0.6 |
| 1880 MHz | 1.9 | 1.5 | 3 | 0.4 |

Fig. 4-18 shows the radiated fields and the radiation pattern for each frequency band. From Figs. 4-18, we can observe a 2.3 dB increase in GSM850 and a 2.1 dB increase in GSM900.

In GSM1900, we observed a 1 dB increase in the radiated field strength. However, for GSM1800, we observed a 1.2dB decrease in the radiated field strength. To explain this degradation, we examined the baseline results and found that the structure is well tuned at the GSM1800 band. The introduction of any matching components adds losses due to the limited quality factor of the components.

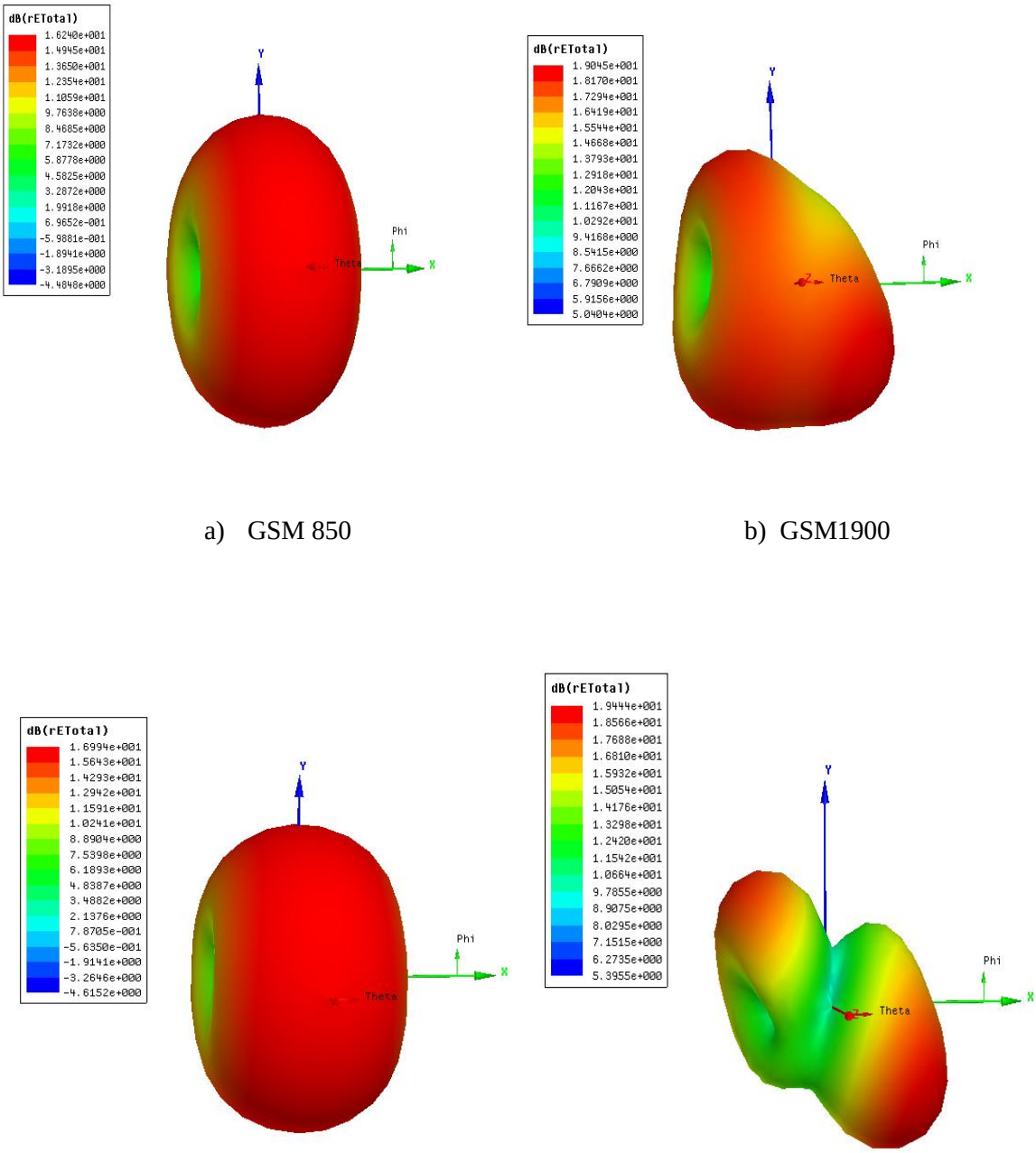


a) GSM 850

b) GSM1900

c) GSM 900

d) GSM1800

Figure 4-18: Radiated fields – Tunable matching network.

## 4.3 Simulation Results Summary and Comparison

### 4.3.1 Summary of Simulation Results – Aperture Tuning

Fig. 4-19 shows the logarithmic magnitude of the antenna return loss ($S_{11}$), captured when inductors and capacitors were connected with the antenna element, as described in sections 4.1.1.2 and 4.1.1.3.

Fig.4-19 clearly shows the effects of series inductors versus series capacitors. We can conclude that adding a series inductor shifts the resonance frequency to a lower value. Hence, it is equal in effect to increasing the physical length of the antenna element, thus helping miniaturize large antenna structures for easier integration in mobile handheld devices [14]. On the other hand, adding a series capacitor shifts the resonance frequency to a higher value.

Table 4-3 shows a comparison between the radiated fields for each value of the tuning element versus the baseline results with the original antenna element. We observed a noticeable performance improvement in the low frequency bands. However, for the high frequency bands, the results do not indicate significant improvement. This can be explained by looking at the baseline measurement, where the antenna is well tuned at the high frequency bands. Thus, adding tuning components will cause losses due to the limited quality factor of such components.

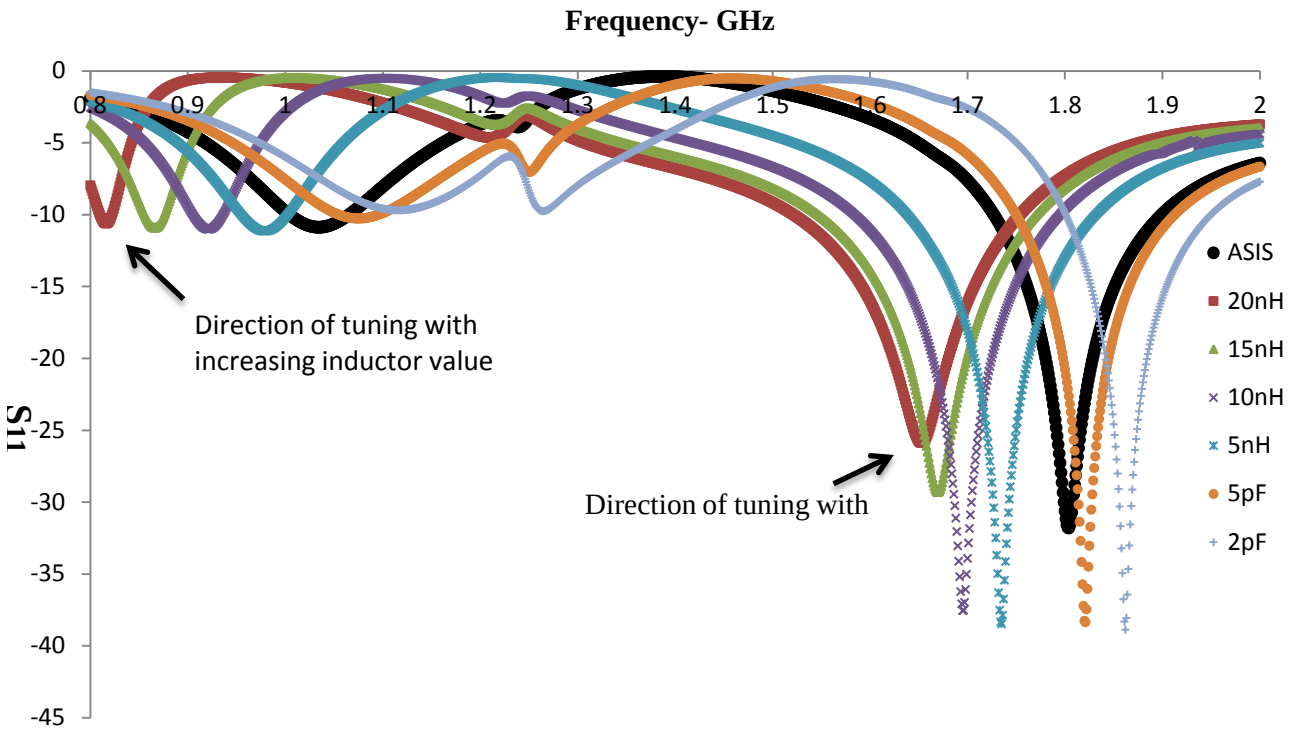


Figure 4-19: Magnitude of the return loss of the antenna in dB – Aperture tuning.

Table 4-3: Peak radiated fields comparison – Aperture tuning.

| Frequency Band | Peak Radiated Field in dB | | | | | | |
|---|---|---|---|---|---|---|---|
| | AS_IS | 20nH | 15nH | 10nH | 5nH | 5pF | 2pF |
| GSM850 | 13 dB | 14.8 dB | 13.73 dB | 13 dB | 12.49 dB | 11.7 dB | 11.2 dB |
| GSM1900 | 18 dB | 18 dB | 18 dB | 18 dB | 18 dB | 18 dB | 18 dB |
| GSM900 | 14.9 dB | 15.8 dB | 16.67 dB | 16 dB | 15.3 dB | 14.4 dB | 13.9 dB |
| GSM1800 | 20.6 dB | 20.1 dB | 20.3 dB | 20.6 dB | 20.7 dB | 20 dB | 18.49 dB |

Table 4-4 shows the antenna parameters for each value of the tuning element. The incident power is fixed to 1 Watt for all cases. It is clearly demonstrated that both the accepted and the radiated power of the antenna change with the changing values of the tuning element.

As an example, the GSM850 antenna accepted power improved from 0.38 W to 0.6512 W. However, from a system point of view, 0.35 W was lost.

Table 4-4: Antenna parameters − Aperture tuning.

| Antenna Parameters | GSM850 | | GSM900 | | GSM1800 | | GSM1900 | |
|---|---|---|---|---|---|---|---|---|
| | Power | | Power | | Power | | Power | |
| | Accepted | Radiated | Accepted | Radiated | Accepted | Radiated | Accepted | Radiated |
| AS_IS | 0.38392 | 0.3279 | 0.58093 | 0.53983 | 0.93988 | 0.92046 | 0.83554 | 0.84851 |
| 20nH | 0.6512 | 0.59236 | 0.88589 | 0.82281 | 0.88006 | 0.86264 | 0.65396 | 0.65643 |
| 15nH | 0.53826 | 0.47982 | 0.87774 | 0.82709 | 0.91057 | 0.89215 | 0.67642 | 0.67971 |
| 10nH | 0.47 | 0.41634 | 0.75815 | 0.71684 | 0.9488 | 0.92943 | 0.70943 | 0.72505 |
| 5nH | 0.42589 | 0.366882 | 0.66504 | 0.61727 | 0.98624 | 0.9554 | 0.75899 | 0.76208 |
| 5pF | 0.36537 | 0.3053 | 0.54749 | 0.49833 | 0.878 | 0.808 | 0.86871 | 0.86782 |
| 2pF | 0.33648 | 0.27627 | 0.49685 | 0.4469 | 0.6659 | 0.5747 | 0.91892 | 0.91285 |

## 4.3.2 Summary of Simulation Results – Tunable Matching Network

Fig. 4-20 shows the logarithmic magnitude of the antenna return loss ($S_{11}$) captured when matching conditions are met at each frequency band. It was clearly demonstrated that we can shift the resonance frequency of the system by changing the values of the lumped capacitors of the matching network.

Table 4-5 shows a comparison (focusing only on the matched band) between the radiated fields for each band when the matching condition is achieved using tunable matching network versus the baseline measurement with fixed matching network. We observed a noticeable performance improvement in the low frequency bands, especially for the GSM850, where the radiated field increased by 3.25 dB. For the GSM 900, the radiated fields improved by 2 dB.

However, for the high frequency bands, the results did not indicate any significant improvement. For the GSM 1900, the radiated fields increased by 1dB, while for the GSM1800, the radiated field decreased by 1.2dB when compared to the baseline measurement. This could be explained by examining the baseline results. For the GSM1800, the antenna structure was well tuned, but we needed to add a matching network to tune the remaining bands, which induced losses.

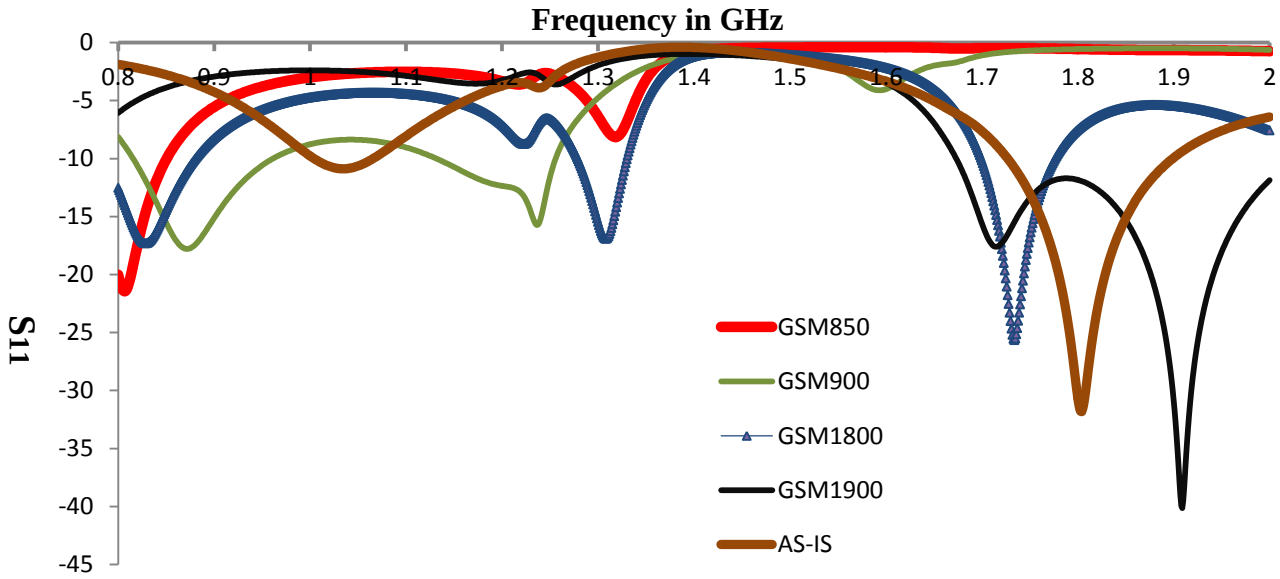


Figure 4-20: Magnitude of the return loss of the antenna in dB – Tunable matching network.

Table 4-5: Peak radiated fields comparison − Tunable matching network.

| Frequency Band | Peak Radiated Field in dB | |
|---|---|---|
| | Original Matching Network | Tunable Matching Network |
| GSM850 | 13 dB | 16.25 dB |
| GSM1900 | 18 dB | 19.04 dB |
| GSM900 | 14.9 dB | 16.9 dB |
| GSM1800 | 20.6 dB | 19.4 dB |

Table 4-6 shows the antenna parameters for each band when the matching condition is achieved. The incident power is fixed to 1 Watt for all cases. It is clearly demonstrated that both the accepted and the radiated power of the antenna were improved.

As an example, the GSM850 antenna accepted power improved from 0.38 W to 0.9823 W, but only 0.848 W was radiated. This is due the added losses of the matching components.

Table 4-6: Antenna Parameters − Tunable matching network.

| Antenna Parameter | GSM850 | | GSM900 | | GSM1800 | | GSM1900 | |
|---|---|---|---|---|---|---|---|---|
| | Power | | Power | | Power | | Power | |
| | Accepted | Radiated | Accepted | Radiated | Accepted | Radiated | Accepted | Radiated |
| AS-IS | 0.3279 | 0.38392 | 0.53983 | 0.58093 | 0.93988 | 0.92046 | 0.84851 | 0.83554 |
| Matched | 0.98233 | 0.84825 | 0.97175 | 0.904 | 0.99 | 0.76 | 0.99 | 0.86 |

### 4.3.3 Comparison of Tunable Matching Network Vs Aperture Tuning

We grouped the data collected from all previous simulations and re-organized it for each band. Fig. 4-21 illustrates a comparison between an aperture-tuned antenna and a matching network-tuned antenna at the GSM850 band. It is clear that the maximum power transfer to and from the antenna occurs when the matching network is tuned to the GSM850 frequency.

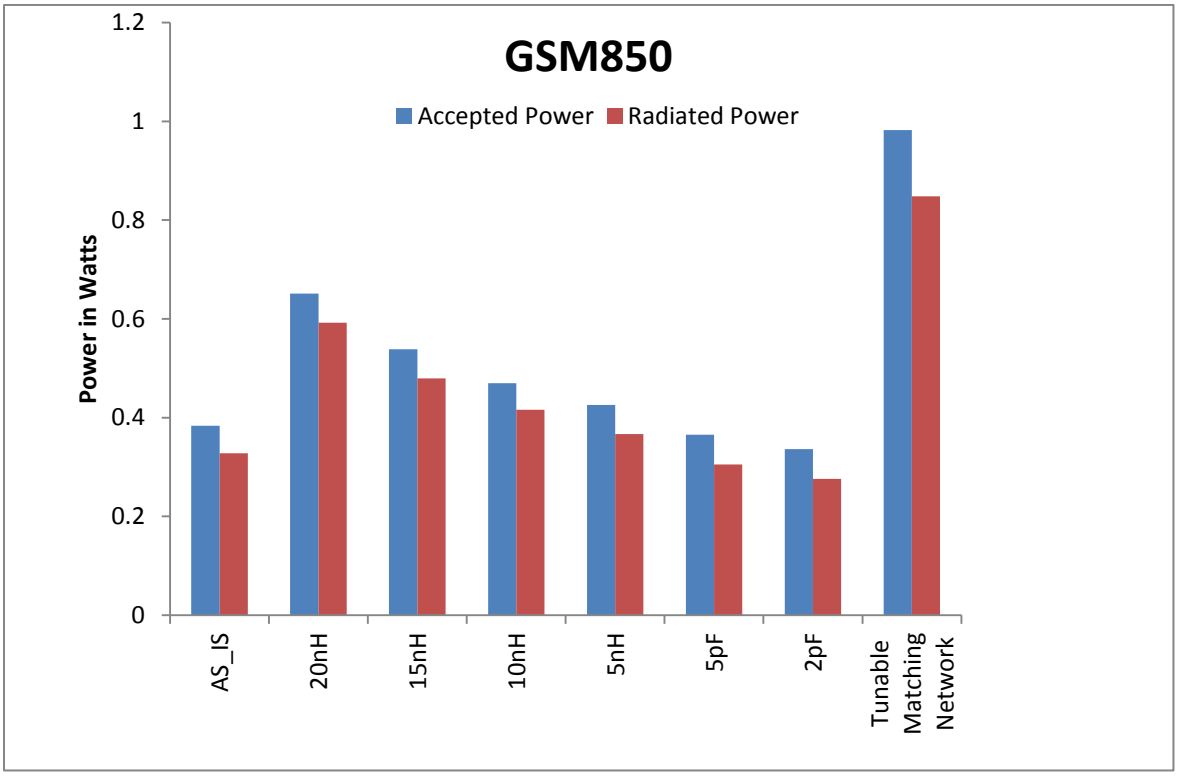


Figure 4-21: GSM850 – Comparison between aperture tuning and tunable matching network.

Fig. 4-22 shows a comparison between an aperture-tuned antenna and a matching network-tuned antenna at the GSM900 band. It can be seen that the maximum power transfer to and from the antenna occurs when the matching network is tuned to the GSM900 frequency.

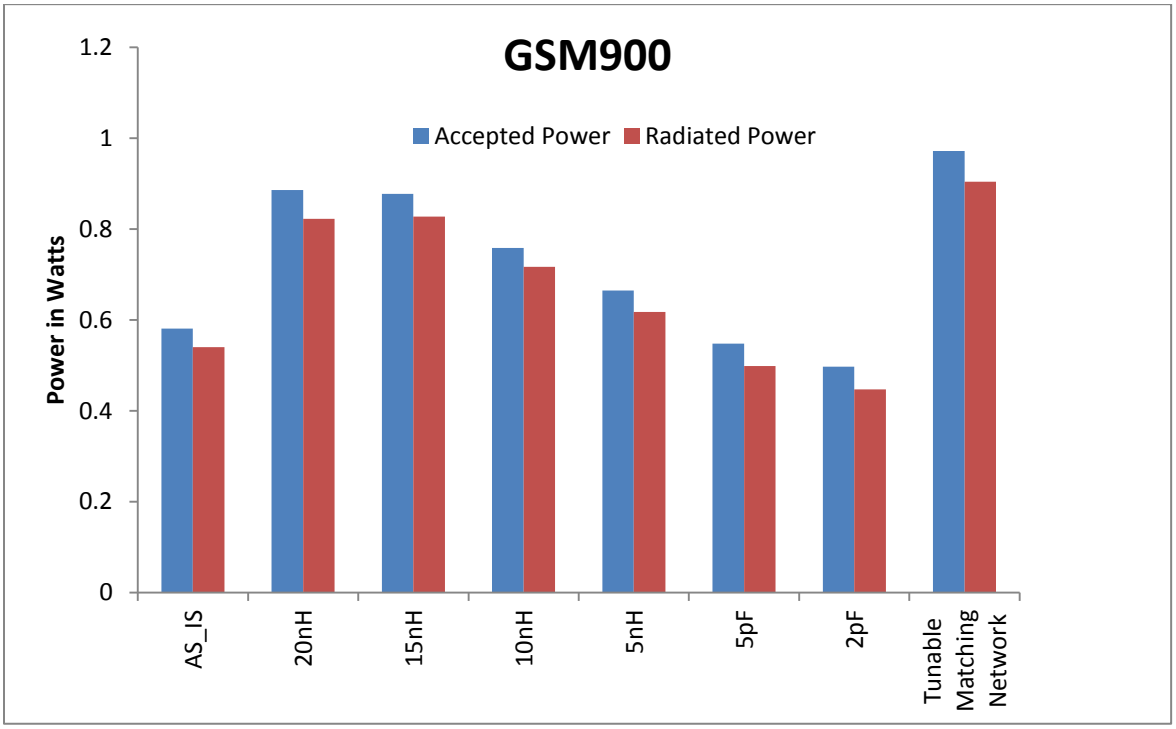


Figure 4-22: GSM900 – Comparison between aperture tuning and tunable matching network.

Fig. 4-23 shows a comparison between an aperture-tuned antenna and a matching network-tuned antenna at the GSM1800 band. It is clear that the maximum power transfer to the antenna occurred when the matching network was tuned to the GSM1800 frequency. However, the maximum power radiated from the antenna occurred when the antenna was tuned with the aperture tuning method. This condition was met when the antenna was tuned with a series 5nH inductor. The reduction in the radiated power was caused by losses introduced by the matching network due to the increased number of components compared to aperture tuning.

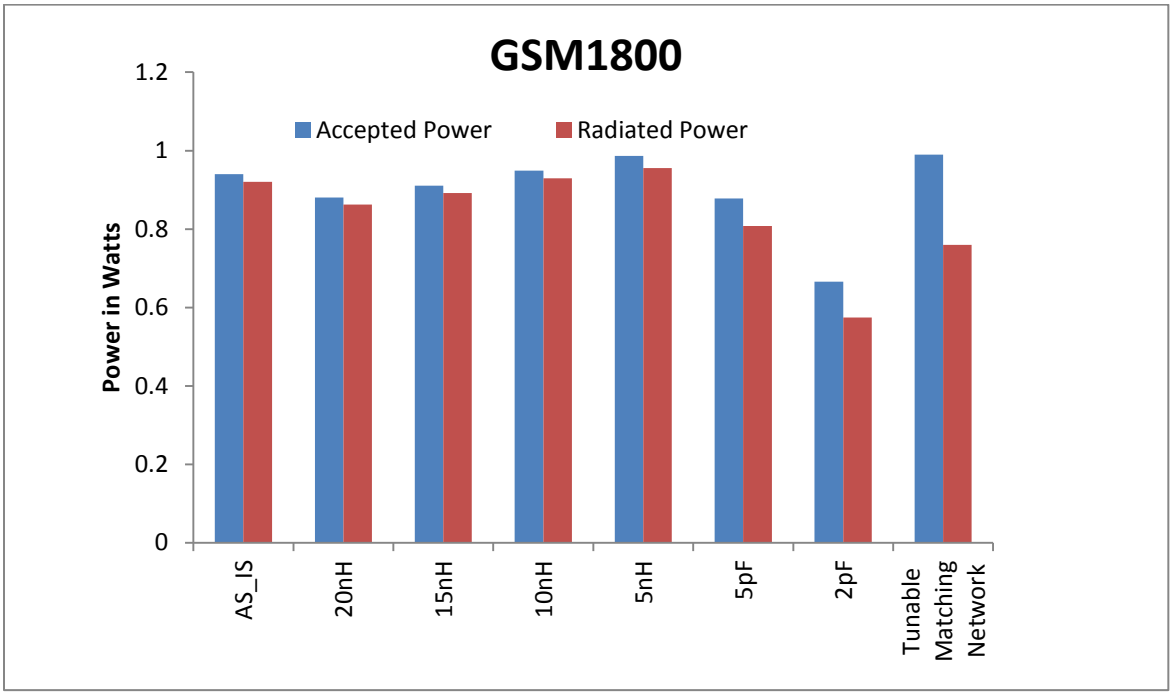


Figure 4-23: GSM1800 – Comparison between aperture tuning and tunable matching network.

Fig. 4-24 shows a comparison between an aperture-tuned antenna and a matching network-tuned antenna at the GSM1900 band. It was demonstrated that the maximum power transfer to the antenna occurred when the matching network was tuned to the GSM1800 frequency. However, the maximum power radiated from the antenna occurred when the antenna was tuned with the aperture tuning method. This condition was met when the antenna was tuned with a series 2pF capacitor. The reduction in radiated power was caused by losses introduced by the matching network due to the increased number of components compared to aperture tuning.

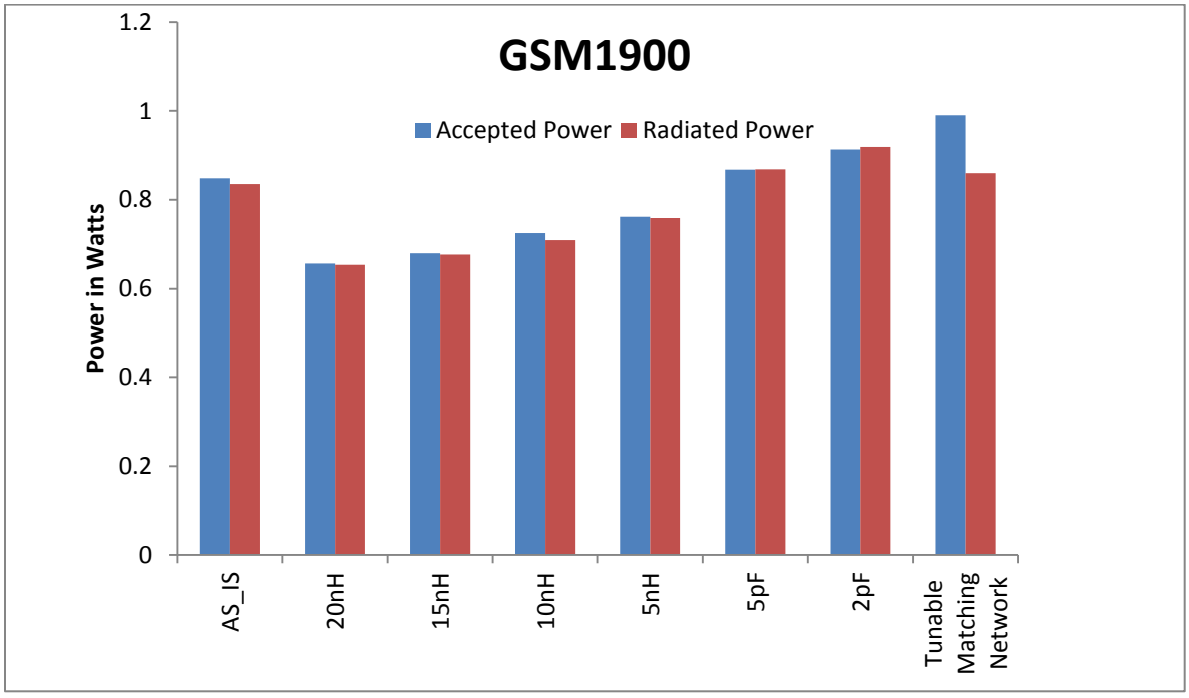


Figure 4-24: GSM1900 – Comparison between aperture tuning and tunable matching network.

## 4.4 Practical Measurement Results

We performed radiated baseline measurements conducted on the M2M device from DBJay Technologies [38]. The device is calibrated according to class 4 for the GSM low band and class 1 for the GSM high band [19] [39].

We measured the conducted power delivered to the antenna. For the GSM850, the conducted power was 32.4dBm, and for the GSM1900, the conducted power was 29.6dBm. The radiated measurement was carried out in an anechoic antenna chamber (model number Dart 3300E) which was designed and manufactured by Tri-Solutions [41].

To be consistent with the industrial measurement standard, we selected two GSM bands for the practical verification, GSM850 and GSM1900. Both bands represent the low and high edge of the covered spectrum.

Table 4-7 shows the comparison results between three cases, the baseline, with aperture tuning and with tunable matching network. Total radiated power captured at the low, middle and high channels of the GSM850. We observed an average of 3dB improvement in the radiated power when a 20nH inductor was used to tune the antenna. We also observed an average of 6 dB improvement when a matching network was tuned for the GSM850 band. This conforms to the simulation results listed in Table 4-4 and Table 4-6. Table 4-8 summarizes a comparison between the calculated results based on simulation and the measured results. The comparison conforms to the trend we expected, based on simulation results

Table 4-7: Measurement results for GSM 850.

| | GSM850-Radiated Power in dBm | | |
|---|---|---|---|
| | Low channel | Mid Channel | High Channel |
| Original Condition | 23.542 | 23.505 | 23.82 |
| Aperture Tuning 20nH | 27.2 | 26.7 | 27.8 |
| Tunable Matching Network-GSM850 | 29.1 | 30.3 | 29.7 |

Table 4-8: GSM850 – Comparison between measurement and simulation results.

| | Measured | | | Calculated from simulation results | | |
|---|---|---|---|---|---|---|
| GSM850 | Baseline | Aperture tuning | Matching Network tuning | Baseline | Aperture tuning | Matching Network tuning |
| Power delivered (dBm) | 32.4 | 32.4 | 32.4 | 32.4 | 32.4 | 32.4 |
| Power accepted (dBm) | N/A | N/A | N/A | 28.2 | 30.4 | 32.2 |
| Power Radiated (dBm) | 23.505 | 26.7 | 30.3 | 23.4 | 28.2 | 31.5 |

Similarly, for the high band, Table 4-9 provides a comparison between the total radiated power captured at the low, middle and high channels of the GSM1900. We observed an average of 0.2dB improvement in the radiated power when 2pF inductor was used to tune the antenna. In this case, we observed no significant change in the radiated power when the matching network was tuned for the GSM1900 band. This conforms to the simulation results listed in Table 4-4 and Table 4-6.

Table 4-9: Measurement results for GSM1900.

| | GSM1900-Radiated Power in dBm | | |
|---|---|---|---|
| | Low channel | Mid Channel | High Channel |
| Original Condition | 27.36 | 28.21 | 28.98 |
| Aperture Tuning 2pF | 28 | 28.5 | 29.2 |
| Tunable Matching Network-GSM1900 | 27.67 | 27.9 | 28.5 |

Table 4-10 summarizes a comparison between the calculated results based on a simulation and the measured results. The comparison conforms to the trend we expected, based on simulation results.

Table 4-10: GSM1900 – Comparison between measurement and simulation results.

| | Measured | | | Calculated from simulation results | | |
|---|---|---|---|---|---|---|
| GSM1900 | Baseline | Aperture tuning | Matching Network tuning | Baseline | Aperture tuning | Matching Network tuning |
| Power delivered (dBm) | 29.6 | 29.6 | 29.6 | 29.6 | 29.6 | 29.6 |
| Power accepted (dBm) | N/A | N/A | N/A | 28.8 | 29.2 | 29.5 |
| Power Radiated (dBm) | 28.21 | 28.5 | 27.9 | 28.1 | 28.8 | 28.8 |

## 4.5 Conclusion

We conducted a detailed study on a practical M2M wireless radio to compare performance differences when using an aperture tuning technique to tune the antenna versus using a switchable matching network.

We modeled the device in HFSS and conducted several simulation runs. Also, for verification, we measured the total radiated power for the practical design when the aperture tuning was used by inserting series tuning elements on the antenna element. For this, we used 20nH to tune the GSM850 and used 2pF to tune the GSM1900.

Similarly, we measured the total radiated power when a switchable matching network is used. We switched the lumped component to achieve matching at each band.

Both measurement and simulation results revealed the following:

- In the low frequency band, the performance with switchable matching network was better than the performance with aperture tuning. This is valid for power accepted and radiated by the antenna.

- In the high frequency band, the power accepted by the antenna was improved in the case of the switchable matching network over the aperture tuning method; however, the power radiated was lower. This is due to losses introduced by the large number of reactive elements used in the matching network.

# Chapter 5

# Conclusion and Future Work

## 5.1 Thesis Conclusion

Handset mobile devices are reaching their intrinsic limitations in terms of the space allowed for integration. This is prompting the necessity for adaptive impedance tuning. In this work, we presented a detailed study of various tuning options.

The contributions of this thesis can be summarized as follows:

1. We carried out simulation of different tuning network topologies to study the tuning range for each one. Our simulation results showed that the low pass Π network is the best candidate for a generic impedance tuning network. From this we can conclude that this toplogy is a good preliminary start for many tunable designs.
2. We illustrated a technique to substitute variable inductors with fixed inductors connected to two tunable capacitors. We showed that the circuit can substitute series inductors in Π networks, with some limitation in the tuning range.
3. We also measured the 2-port network parameters of a commercially available BST capacitor. From the measurement, we extracted the equivalent circuit and the quality factor of the BST capacitor. The quality factor of the measured BST capacitors ranged from 90 to 30 when the bias voltage swept from 2 to 20V. This is much lower than the quality factor of many available lumped capacitors, leading us to conclude that adaptability comes with the penalty of higher losses.
4. We conducted a study to compare two different methods of tuning: a) aperture tuning and b) matching network tuning. We modeled commercially available mobile device antenna in an HFSS EM simulator. The study results showed that, with tunable matching networks, the power accepted by the antenna is improved over the aperture tuning method; however, the radiated power was lower in certain bands although the antenna

performance was acceptable. The reduction of the radiated power is related to the limited quality factor of the tuning elements.

5. We carried out extensive simulations to prove that tuning comes with benefits at some frequency bands where the antenna performance is poor. In these cases, the mismatch losses of the antenna were higher than the insertion losses of the tunable components.
6. We conducted practical verification using total radiated power measurements on the physical device used in the simulation. Both measurement and simulation results followed the same trend.

## 5.2 Future Work

In our future work, we will focus on investigating different tuning elements, including switchable capacitor banks, BST devices and MEMS devices. We will also study possible means of switching matching networks in and out or perhaps bypassed. This is to avoid added losses where possible.

We will also investigate hybrid solution that combines both tuning techniques. Wherein the aperture tuning method can be used for high frequency bands and the tunable matching networks can be used for low frequency bands.

As well, we will work on methods to estimate the change of antenna impedance caused by user interaction. Ideally, this needs to be done without adding RF detectors or directional couplers, as the addition of components will induce added losses [44]. In the next section, we will illustrate the motivation of our future work.

### 5.2.1 Effect of user interaction on mobile wireless devices antenna

Power is lost due to mismatches between the radio's front-end module and the antenna. Minimizing losses is the main target of any RF design team, which can be very challenging on its own. The complexity of this task increases when the load impedance is a moving target. To illustrate, we measured the antenna impedance for a BlackBerry smart phone (BB9100). The free

space antenna impedance is shown in Fig. 5-1(a) and the user interaction antenna impedance is shown in Fig.5-1 (B). We can observe that, in some cases, the change in both the magnitude and phase of the impedance is severe.

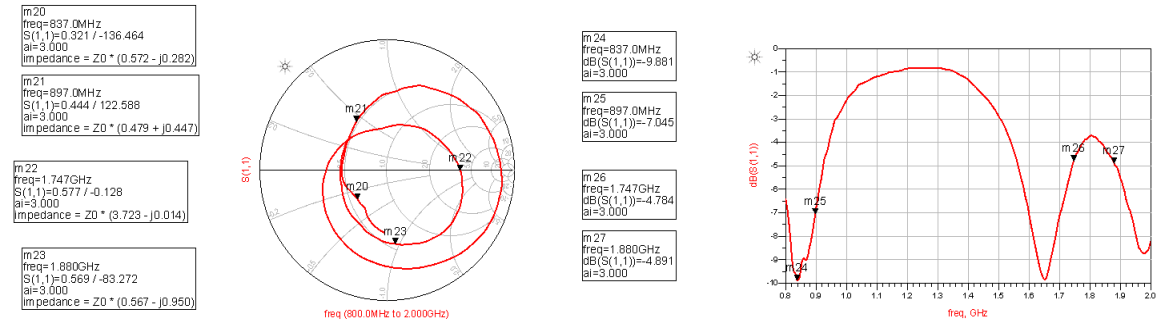


a) Free Space

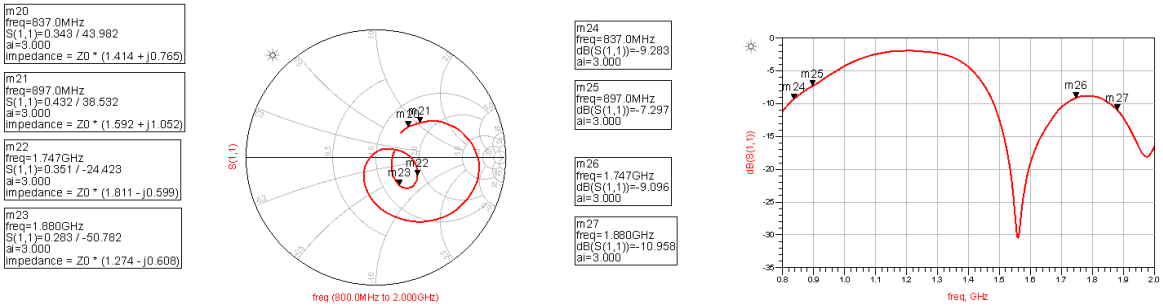


b) User Typing on Keyboard

Figure 5-1: Blackberry 9100 measured antenna impedance.

After factoring in the linearity, output power, and wide frequency coverage and modulation mechanism requirements of the RF power amplifier, user interaction will change both the magnitude and phase of the antenna impedance. This would be reflected as a difference in the impedance seen by the RF PA.

The RF PA is a nonlinear active device. The power available to the load will change based on the load impedance. This fact can be better explained if the load pull behavior of the PA is

studied. To illustrate, we measured the load-pull characteristics of a Skyworks 77526 RF power amplifier. Fig.5-2 shows the load-pull measurement with the change of the antenna impedance due to handling mapped on it. We observed the power delivered to the antenna changed by more than 1.25dB due to user interaction. This is not linearly changing with changes in the real part of the antenna impedance.

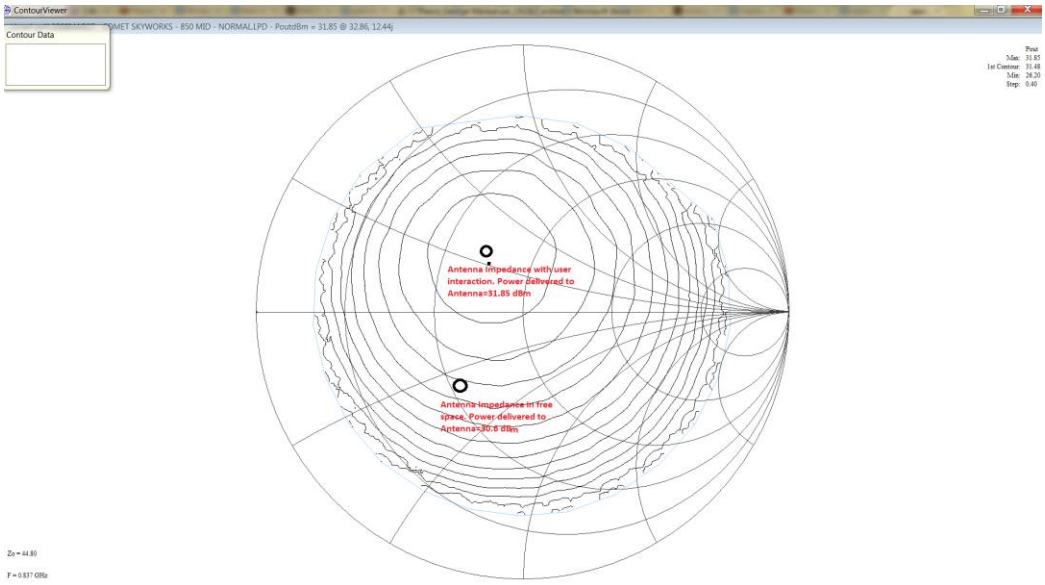


Figure 5-2: Load-pull measurement for Skyworks RF PA with antenna load change due to handling.

User interaction scenarios are unlimited and heavily dependent on each user. For example, devices can be held tightly in the hand and or held against a face. Users could be wearing gold jewelry or glasses, or could even have crowns in their teeth. Hence, it is impossible for designers to account for all handling scenarios without adaptive impedance tuning.

Wireless carriers became aware of these issues and accordingly revised their specifications on TRP (Total Radiated Power) and TIS (Total Isotropic Sensitivity) to include handling effects. For example, it was sufficient for handheld mobile devices to possess TRP/TIS in free space conditions. The carriers then moved to add head phantom specifications [9], which is about 6 dB

lower than the mobile free space reading. These values are chosen to account for the absorption that occurs in the human head. However, it does not account for changes in the power delivered due to changes in antenna impedance. Subsequently, they added hand effects, which further complicated the design process.

In order to offset losses caused by handling, RF engineers cannot simply increase the power delivered to the antenna, as the RF PAs must be calibrated to a specified power output, as required in 3GPP specifications. For example, a GSM phone is calibrated for a maximum of 33dBm output power.

Moreover, from a design quality point of view, RF engineers must make sure that wireless mobile devices will operate linearly even at lower battery voltages. They cannot simply mitigate these issues by increasing the calibrated output power, as the linearity requirements of the system would be the limiting factor.

From the device certification point of view, even if there is room to increase the power delivered to the antenna, there might be an impact on FCC certification. For example, a higher output power can produce higher harmonic emissions and can also increase the difficulty of passing the Specific Absorption Rate (SAR) specification.

Our future work will revolve around researching different techniques to mitigate the aforementioned issues by adaptively tuning antenna impedance.

# Bibliography


[1] "PTCRB Certification," [Online]. Available: http://www.cetecom.com/us/en/certification/north-america/ptcrb.html.

[2] E. Ofli, C.H Li, N. Chavannes, N. Kuster, "Analysis and Optimization of Mobile Phone Antenna Radiation Performance in the Presence of Head and Hand Phantoms," *Turkish Journal of Electrical Engineering & Computer Sciences*, pp. 2763 - 2770, 2008.

[3] K. R. Boyle, Y. Yuan and L. P. Ligthart, "Analysis of Mobile Phone Antenna Impedance Variations With User Proximity," *ANTENNAS AND PROPAGATION*, vol. 55, no. 2, pp. 364-372, 2007.

[4] "TAF," [Online]. Available: http://www.taf.org.cn/(S(osy5bggfpr4cp4pskamb2lln))/EN/ETAF.ASPX.

[5] AT&T, "Hardware Development – Best Practices to Provide Successful Outcomes," 2011.

[6] Mar. 1996. [Online]. Available: www.etsi.org. [Accessed 03 06 2013].

[7] Office of Engineering and Technology-FCC, "UNDERSTANDING THE FCC REGULATIONS FOR LOW-POWER, NON-LICENSED TRANSMITTERS," OET BULLETIN NO. 63, Washington, DC 20554, 1996.

[8] "www.ecfr.gov," [Online]. Available: http://www.ecfr.gov/cgi-bin/text-idx?c=ecfr&SID=09f0d877b8c3a36eaa4ba31e27b80295&rgn=div8&view=text&node=47:1.0.1.1.16.2.234.6&idno=47.

[9] "http://www.ctia.org/," January 2011. [Online]. Available: http://files.ctia.org/pdf/CTIA_OTA_Test_Plan_Rev_3.1.pdf. [Accessed 03 06 2013].

[10] Okano, Y. , D. Kurita, S. Nakamatsa, T. Okada, "Evaluation of OTA Performance for Mobile Terminal Antenna Reflecting Practical Usage and Improvement of Measurement Efficiency," NTT Docomo, Tokyo, 2011.

[11] S. I. Al-Mously and M. M. Abousetta, "User's Hand Effect on TIS of Different GSM900/1800 Mobile Phone Models Using FDTD Method," in *World*

*Academy of Science, Engineering and Technology*, 2009.

[12] A. van Bezooijen, R. Mahmoudi and A. H. M. van Roermund, "Adaptive Methods to Preserve Power Amplifier Linearity Under Antenna Mismatch Conditions," *CIRCUITS AND SYSTEMS,* vol. 52, no. 10, pp. 2101-2108, 2005.

[13] "White paper, Key Element to Lower Operating Costs While Improving Wireless Network Performance," in *IWPC International Wireless Industry Consurtium*, 2011.

[14] S. Ali, "Tunable Antenna: Theory and Techniques".

[15] F. Domingue, A. B. Kouki and R. R. Mansour, "Improved Distributed MEMS Matching Network for Low Frequency Applications Using a Slow-Wave Structure," in *Microwave Symposium Digest*, Atlanta, 2008.

[16] T. V. Heikkilä, ,. J. Varis, J. Tuovinen and G. M. Rebeiz, "A 20–50 GHz RF MEMS Single-Stub Impedance Tuner," *IEEE MICROWAVE AND WIRELESS COMPONENTS LETTERS,* vol. 15, no. 4, pp. 205-207, 2005.

[17] A. v. Bezooijen, M. A. de Jongh, C. Chanlo, L. C. H. Ruijs, F. v. Straten, R. Mahmoudi and A. H. M. van Roermund, "A GSM/EDGE/WCDMA Adaptive Series-LC Matching Network Using RF-MEMS Switches," *IEEE JOURNAL OF SOLID-STATE CIRCUITS,* vol. 43, no. 10, pp. 2259-2268, 2008.

[18] M. A. De Jongh, A. v. Bezooijen, K. R. Boyle and T. Bakker, "Mobile Phone Performance Improvements using an Adaptively Controlled Antenna Tuner," 2011.

[19] "GSM Techinical Specifications," ETSI, Valbonne-Frace, 1996.

[20] ETSI, [Online]. Available: http://www.etsi.org/standards.

[21] H. Holma and A. Toskala, in *WCDMA for UMTS*, Wiley, 2007, pp. 588-890.

[22] J. Brank, J. Yao, M. Eberly, A. Makczewski, K. Varian and C. Goldsmith, "RF MEMS-Based Tunable Filters," *International Journal of RF and Microwave Computer-Aided Engineering*, pp. 276-284, 2001.

[23] G. M. Rebeiz, K. Entesari, I. C. Reines, S.-J. Park, M. A. El-Tanani, A. Grichener and A. R. Brown, "Tuning In RF MEMS," pp. 55-72, October 2009.

[24] M. A. El-Tanani and G. M. Rebeiz, "High-Performance 1.5–2.5-GHz RF-MEMS Tunable Filters for Wireless Applications," *IEEE TRANSACTIONS ON MICROWAVE THEORY AND TECHNIQUES,* vol. 58, pp. 1629-1637, 2010.

[25] M. Rahman and K. Shamsaifer, "Electronically Tunable LTCC Based Multi Layer Filter For Mobile Handset Application," *IEEE MTT-S Digest,* pp. 1767-1770, 2003.

[26] V.-A. Nguyen, R. A. Bhatti and S. O. Park, "A Simple PIFA-Based Tunable Internal Antenna for," *IEEE Antenna and Propagation,* vol. 7, pp. 130-133, 2008.

[27] Ma-Com Technology Solution, "Macom-datasheets," [Online]. Available: https://www.macomtech.com/datasheets/MA46H120.pdf. [Accessed 25 July 2013].

[28] W. C. E. Neo, Y. Lin, ,. X.-d. Liu, L. C. N. de Vreede, L. E. Larson, M. Spirito, M. J. Pelk, K. Buisman, A. Akhnoukh, A. de Graauw and L. K. Nanver, "Adaptive Multi-Band Multi-Mode Power Amplifier Using Integrated Varactor-Based Tunable Matching Networks," *IEEE JOURNAL OF SOLID-STATE CIRCUITS,,* vol. 41, no. 9, pp. 2166-2176, 2006.

[29] "Murata Components Library for Agilent ADS," Murata, May 2012. [Online]. Available: http://www.murata.com/products/design_support/agilent/index.html.

[30] A. van Bezooijen, A. M. de Jongh, F. van Straten, R. Mahmoudi and A. H. M. van Roermund, "Adaptive Impedance-Matching Techniques for Controlling L Networks," *IEEE-Circuits and Systems,* vol. 57, no. 2, pp. 495-505, 2010.

[31] R. Whatley, T. Ranta and D. Kelly, "CMOS Based Tunable Matching Networks for Cellular Handset Applications," in *Microwave Symposium Digest (MTT),* Baltimore, 2011.

[32] A. Tombak, "A Ferroelectric-Capacitor-Based Tunable Matching Network for Quad-Band Cellular Power Amplifiers," *Microwave Theory and Techniques,* vol. VOL. 55, no. 2, pp. 370-375, 2007.

[33] A. Tombak, J. P. Maria, F. Ayguavives, Z. Jin, G. T. Stauf, A. I. Kingon and A. Mortazawi, "Tunable Barium Strontium Titanate Thin Film Capacitors for RF

and Microwave Applications," *IEEE MICROWAVE AND WIRELESS COMPONENTS,* vol. 12, no. 1, pp. 3-5, January 2002.

[34] On Semiconductor, 05 2013. [Online]. Available: http://www.onsemi.com/pub_link/Collateral/TCP-3047H-D.PDF. [Accessed 10 09 2013].

[35] D. M. Pozar, in *Microwave Engineering*, John Wiley & Sons, Inc., 2005, pp. 170-187.

[36] Agilent, *Advanced Design System 2012.08.*

[37] Murata , "Simsurfing," [Online]. Available: http://ds.murata.co.jp/software/simsurfing/en-us/index.html. [Accessed 01 09 2013].

[38] DBJay Technologies Inc., [Online]. Available: http://www.dbjtech.com/pro.php?head=2&id=15.

[39] Third Generation Patnership 3GPP, "Digital cellular telecommunications system, Physcial Layer on the Radio Path Technical Specification V4.0.1-DTS/TSGG-0145001Uv4," Sophia Antipolis Cedex, Nice, 2000.

[40] Ansoft Corporation, *Ansoft HFSS V10.0.*

[41] Tri L. Soluations, [Online]. Available: http://www.trilsolutions.com/?p=84.

[42] Murata, "Murata Chip Inductor Datasheet," [Online]. Available: http://www.murata.com/products/catalog/pdf/o05e.pdf. [Accessed 01 09 2013].

[43] F. Dellsperger and M. Baud, "Smith 3.10," June 2010. [Online]. Available: http://www.fritz.dellsperger.net/.

[44] G. S. Mankaruse, G. Shaker, S. B. Simmons and P. Jarmuszewski, "Mobile wireless communications device including acoustic coupling based impedance adjustment and related methods". USA - Canada Patent CA2788747 A1, 05 09 2012.